Bull Volcanol (1992) 54:126-146

Bulletin of
Volcanology

Mount St. Helens a decade after the 1980 eruptions: magmatic models, chemical cycles, and a revised hazards assessment

John S Pallister[1], **Richard P Hoblitt**[2], **Dwight R Crandell**[1], **and Donal R Mullineaux**[1]

[1] US Geological Survey, Box 25046, MS 903, DFC, Denver, CO 80225, USA
[2] US Geological Survey, Cascades Volcano Observatory, 5400 MacArthur Blvd, Vancouver, WA 98661, USA

Received August 8, 1990/Accepted June 28, 1991

Abstract. Available geophysical and geologic data provide a simplified model of the current magmatic plumbing system of Mount St. Helens (MSH). This model and new geochemical data are the basis for the revised hazards assessment presented here. The assessment is weighted by the style of eruptions and the chemistry of magmas erupted during the past 500 years, the interval for which the most detailed stratigraphic and geochemical data are available. This interval includes the Kalama (A.D. 1480-1770s?), Goat Rocks (A.D. 1800-1857), and current eruptive periods. In each of these periods, silica content decreased, then increased. The Kalama is a large amplitude chemical cycle (SiO_2: 57%-67%), produced by mixing of arc dacite, which is depleted in high field-strength and incompatible elements, with enriched (OIB-like) basalt. The Goat Rocks and current cycles are of small amplitude (SiO_2: 61%-64% and 62%-65%) and are related to the fluid dynamics of magma withdrawal from a zoned reservoir. The cyclic behavior is used to forecast future activity. The 1980-1986 chemical cycle, and consequently the current eruptive period, appears to be virtually complete. This inference is supported by the progressively decreasing volumes and volatile contents of magma erupted since 1980, both changes that suggest a decreasing potential for a major explosive eruption in the near future. However, recent changes in seismicity and a series of small gas-release explosions (beginning in late 1989 and accompanied by eruption of a minor fraction of relatively low-silica tephra on 6 January and 5 November 1990) suggest that the current eruptive period may continue to produce small explosions and that a small amount of magma may still be present within the conduit. The gas-release explosions occur without warning and pose a continuing hazard, especially in the crater area. An eruption as large or larger than that of 18 May 1980 (~ 0.5 km^3 dense-rock equivalent) probably will occur only if magma rises from an inferred deep (≥ 7 km), relative large (5-7 km^3) reservoir. A conservative approach to hazard assessment is to assume that this deep magma is rich in volatiles and capable of erupting explosively to produce voluminous fall deposits and pyroclastic flows. Warning of such an eruption is expectable, however, because magma ascent would probably be accompanied by shallow seismicity that could be detected by the existing seismic-monitoring system. A future large-volume eruption (≥ 0.1 km^3) is virtually certain; the eruptive history of the past 500 years indicates the probability of a large explosive eruption is at least 1% annually. Intervals between large eruptions at Mount St. Helens have varied widely; consequently, we cannot confidently forecast whether the next large eruption will be years, decades, or farther in the future. However, we can forecast the types of hazards, and the areas that will be most affected by future large-volume eruptions, as well as hazards associated with the approaching end of the current eruptive period.

Introduction

Even before the catastrophic eruption of 18 May 1980, Mount St. Helens was known to be frequently active and explosive and was regarded as the most dangerous volcano in the Cascade Range of the western United States. Crandell and Mullineaux (1978) concluded that 'In the future, Mount St. Helens probably will erupt violently and intermittently just as it has in the recent geologic past, and these future eruptions will affect human life and health, property, agriculture, and general economic welfare over a broad area'. These statements were confirmed by the paroxysmal eruption of 18 May 1980, and remain valid today.

The hazards assessment presented here is based primarily on a portion of the eruptive history of the volcano and assumes that types, scales, and effects of future eruptions will be similar to those that have occurred in the past. An earlier assessment (Crandell and Mullineaux 1978) considered events during the Spirit Lake eruptive stage, a series of intermittent eruptive pe-

Offprint requests to: JS Pallister

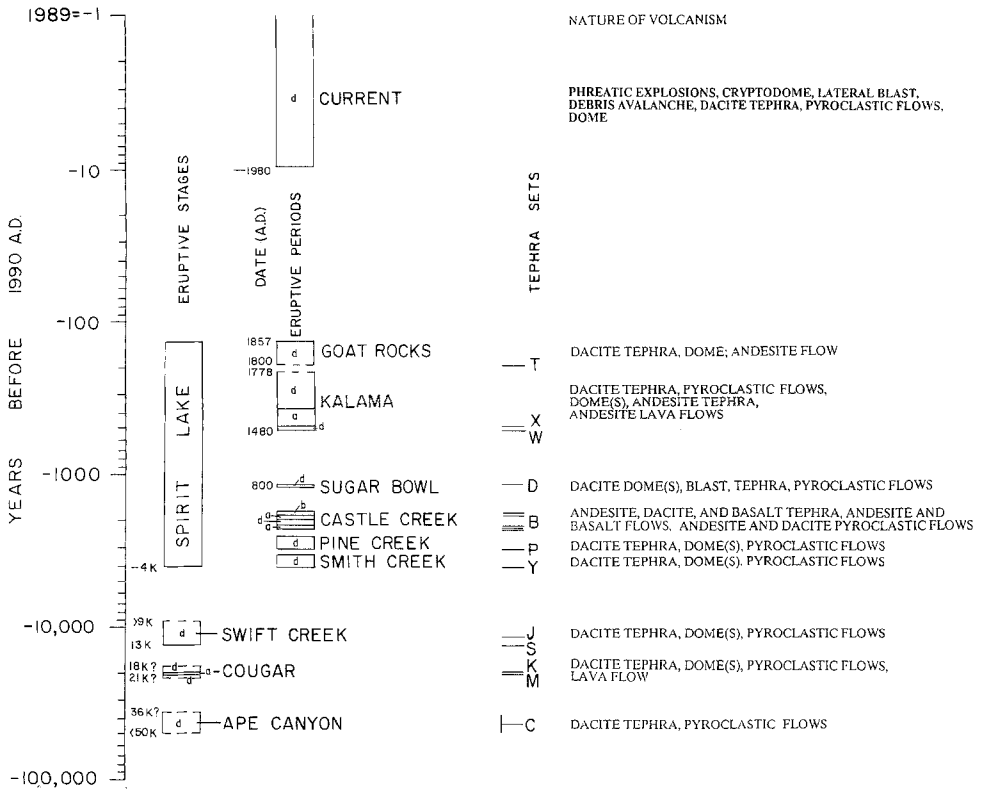

Fig. 1. Eruptive history of Mount St. Helens. Data from Crandell (1987) and Hoblitt (1989). Symbols: *K*, thousand years; *d*, dacite; *a*, andesite; *b*, basalt

riods that began about 4000 years ago and that was preceded by a dormant interval of about 6000 years (Fig. 1). In this reassessment we focus on events of the past 500 years - the Kalama, Goat Rocks, and current eruptive periods - which were preceded by a dormant interval of 600 to 700 years.

Even though, at this writing (1990–1991), Mount St. Helens has been relatively inactive for more than four years, we cannot be sure the eruptive period that began in 1980 has ended. In order to assess the possibility of further eruptions within the next few decades, we review the present status of the volcano and its eruptive history during the past 500 years. We then forecast potentially hazardous events that could occur either if the behavior pattern of the last several years continues, or if a large volume of magma again moves upward from a deep magma reservoir. Our reassessment (1) critically reviews what is known and inferred about the 1980-present magma system, (2) discusses the eruptive events and variation in chemistry of magmas produced during the past 500 years, and (3) forecasts future activity and summarizes the status of hazard zonation at the volcano.

The 1980-to-present conduit and magma reservoir: a critical review

A deep magma reservoir

Several independent lines of evidence indicate that the eruption of 18 May 1980 was fed from a magma body whose top was about 7 km below the present crater floor. Deformation and seismic data were used by Scandone and Malone (1985) to determine the depth of the magma reservoir. Maximum subsidence of the volcano, which amounted to 0.7 m during the six months following the eruptions of 18 May, was modeled by extraction of 0.15–0.24 km^3 of magma from a depth of 7 to 9 km, assuming elastic response of the crust. Hypocenters for earthquakes that followed the eruptions of 18 May, 25 May, and 12 June 1980 enclose an earthquake-free zone believed to be the magma reservoir (Fig. 2). 'The top of this zone is at a depth of about 7 km, it has an average diameter of about 1.5 km and a vertical extent of 6 km or more. This would give a minimum volume of about 10 km^3' (Scandone and Malone 1985). Tomographic inversion of earthquake data from the Mount St. Helens area defines a low-velocity anomaly beneath the crater at depths of 6 to 16 km, which corresponds closely to the depth interval of the earthquake-free zone and is interpreted as a zone of magma accumulation (Lees and Crosson 1989). Recent seismic studies (Malone 1990; Barker and Malone in press) have refined the magma reservoir model. Pressure and tension axes from focal mechanism solutions for earthquakes that followed the 18 May and 12 June eruptions form a circular pattern centered on the aseismic volume. The data are modeled as resulting from magma withdrawal from a cylindrical body located 600 m north of the current dome at depths of 7 to 11 km; the inferred magma body has a radius of 0.65 to 0.75 km and a volume of 5 to 7 km^3.

Data from phase equilibria experiments also constrain the depth and physical conditions of the magma reservoir (Rutherford et al. 1985; Rutherford and Devine 1988). Pumice erupted on 18 May contains pheno-

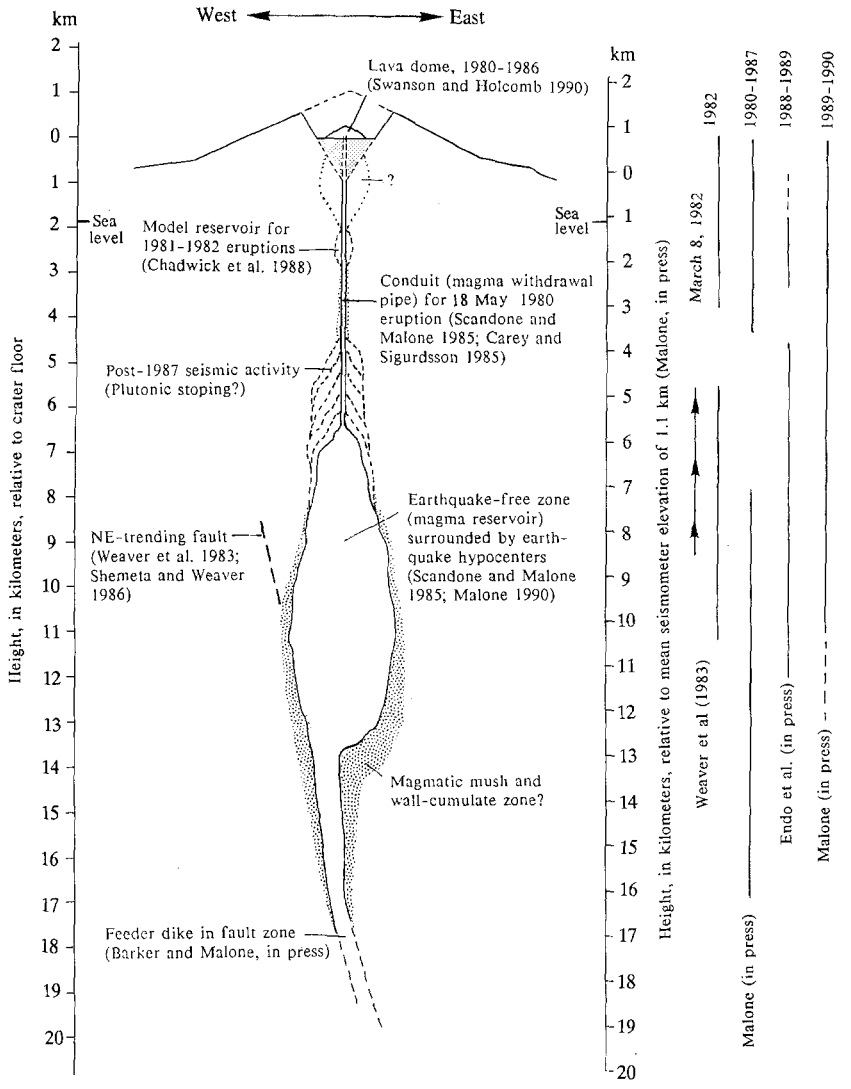

Fig. 2. Inferred Mount St. Helens magmatic plumbing system in east-west cross section. Adapted from Malone (1990), Scandone and Malone (1985) and Rutherford et al. (1985). Columns on right indicate depth intervals of seismicity (*solid lines*) and seismic gaps (*breaks in lines*) for indicated periods of time. *Arrowheads* indicate migration of seismicity on 8 March 1982. *Question mark* indicates hypothetical stock inferred by Casadevall et al. (1983) from sulfur data (see text for critique)

crysts of plagioclase, orthopyroxene, amphibole, Ti-magnetite, and ilmenite. Melt inclusions in plagioclase contain 70% SiO_2 and $4.6 \pm 1\%$ volatiles (determined by difference). The phase assemblage was reproduced experimentally by Rutherford and Devine at f_{O_2} between NNO and $MnO\text{-}Mn_3O_4$. Amphibole and the other phases (including An_{49} plagioclase) were produced at X_{H_2O} in the fluid of 0.67 ($P_{fluid} = 220$ MPa, $T = 920°$ C). The average dissolved volatile content of the experimental glasses is $5.0 \pm 0.4\%$, equivalent to the volatile content of melt inclusions in natural amphibole phenocrysts ($5.0 \pm 0.5\%$, by difference) and overlapping with that in the plagioclase inclusions. The experimental data suggest that the upper part of the magma chamber was at 220 ± 30 MPa, equivalent to a depth of 7.2 ± 1 km, just prior to eruption.

Magma ascent, conduit size and reservoir depth: the effects of uncertainties in eruptive volumes and arrival times

Several studies have used estimates of the volume of juvenile magma and the time of its arrival at the surface to calculate ascent rates and apparent conduit radii for the 18 May eruptions. In the following section, we reevaluate these model calculations and the subsidence model for source depth in the light of new data that suggest potentially large uncertainties in the estimates of eruptive volumes and arrival times.

A magma-ascent velocity (v_S) of 0.6–0.7 m s^{-1} (2.2–2.5 km h^{-1}) was calculated by Scandone and Malone (1985), based on the assumption that the ascent time corresponds to the 3½-h interval between the onset of the first and second phases of ground shaking accompanying the 18 May eruptions (i.e. 0832 until about 1200 PDT). Using the ascent velocity, and a magma supply rate (MSR) derived from volumes and durations of eruptions on 18 May, Scandone and Malone calculated an average effective radius of the conduit of 50–55 m from the formula for flow through a cylindrical conduit.

It has generally been assumed that eruptions during the morning of 18 May first tapped cryptodome magma, then conduit-resident magma, and that the second phase of ground shaking and accompanying color change of the eruption column to light gray at about noon recorded arrival of new magma from the deep (>7 km) chamber. However, Criswell (1987) attributes

the color shift to a change in the eruptive process and incorporation of fine-grained ash that was elutriated from pyroclastic flows. Criswell suggests a first arrival of magma from the deep chamber during the preceding early Plinian phase of the eruption (0900–1215 PDT), despite the dominantly shallow (<3 km) seismicity that accompanied this eruptive phase (Shemeta and Weaver 1986). Accordingly, there is some uncertainty in choosing the arrival time for magma from depth and, therefore, in the derivative ascent velocities. We suspect that melt remaining in the conduit system from feeding of the cryptodome was erupted during the morning hours of 18 May and may represent the early juvenile component of Criswell (1987). Endmember calculations using ascent times of 3.5 h (0832–1200) and 0.5 h (0832–0900) result in a velocity range of 0.6–4.0 m s^{-1} for ascent from 7 km depth. Buoyancy and viscosity relations suggest that the ascent velocity was near the low end of this range (Carey and Sigurdsson 1985), consistent with the interpretation that juvenile magma erupted prior to noon was already present in the conduit.

The volume (expressed as dense-rock equivalent, DRE) of 18 May magma has also proven difficult to determine accurately. The total volume 0.189 km^3 (Lipman et al. 1981b) used by Scandone and Malone in calculating MSR is probably too low (uncertainties of 20–50% were suggested by Scandone and Malone). More complete thickness data for distal tephra increase the juvenile magma estimate (excluding the blast deposit) to 0.242 km^3 (Carey and Sigurdsson 1985). Using this figure and an ascent velocity of 1 m s^{-1}, Carey and Sigurdsson calculated a conduit radius of 47 m from the MSR equation. However, recent stratigraphic work on the 18 May deposits by Criswell (1989) indicates that the total volume for 18 May should be increased to approximately 0.5 km^3, of which 0.33 km^3 represents the Plinian phase of the eruption. The net effect of additional corrections for lithic components, which are more abundant than previously recognized, and possibly a larger volume of flow deposits and tephra (Criswell, personal communication 1990) could either decrease or increase the estimate of juvenile magma volume.

Considering the uncertainties, we believe that the juvenile magma volume erupted on 18 May was probably within the range 0.2 to 0.4 km^3 (DRE) and that these data can only be used to estimate *ranges* for the average MSR and effective conduit radius for the 18 May Plinian eruptions. Dividing the volumes by 9 h (0900–1800 PDT) yields an average MSR range of 6000–12000 m^3 s^{-1}; these values of MSR and $v_S = 1$ m s^{-1} (Carey and Sigurdsson 1985) yield an effective conduit radius range of 30–60 m.

We can also reevaluate the effect of the uncertainties on the estimation of magma reservoir depth from deformation data using the same elastic response model for removal of volume from a point source at depth as used by Scandone and Malone (1985):

$$c = \left[\frac{\delta V(1-\nu)}{\pi h}\right]^{\frac{1}{2}}$$

where h is the vertical deformation, δV is the volume decrease at the source, ν is the Poisson ratio (0.25), and c is depth of the source.

Substituting the range in values for maximum subsidence of the volcano for the period mid June to late November 1980 (0.2 to 0.7 m, Swanson et al. 1981), and our estimate of the probable volume range of 0.2 km^3 to 0.4 km^3 for juvenile magma, yields 8 to 22 km for depth to source. The minimum depth results from maximizing subsidence ($h = 0.7$ m) and minimizing magma volume ($\delta V = 0.2$ km^3); thus, we regard 8 km as the minimum solution for depth to source, providing the assumptions in the elastic response model are correct. These include the following: (1) that subsidence was complete by November 1980; (2) that our estimate of 0.2 to 0.4 km^3 for magma erupted during the afternoon of 18 May is appropriate for modeling subsidence over the period June–November 1980; and (3) that extraction of magma from depth can be modeled by uniform collapse of a body at depth ('uniform negative dilatation of a point source', Walsh (1975)).

The uncertainty in estimation of erupted volumes has a large effect on calculated depth. Because most estimates of eruptive volumes are probably low (Criswell 1987, 1989) correction of these estimates are likely to increase rather than decrease calculated depth. For example, if we hold the maximum subsidence at 0.7 m and increase the total volume estimate from 0.2 to 0.4 km^3, the minimum depth changes from 8 to 12 km.

A second uncertainty involves the relation of subsidence to deep magma withdrawal. Vertical angle measurements, made after November 1980, indicate that subsidence was complete by early 1981 and that the estimate of 0.2 to 0.7 m is approximately correct (Swanson et al. 1981). Although the magmatic 'plumbing' system below Mount St. Helens is probably much more complex in detail than the simplified model shown in Fig. 2, the volume of magma erupted in 1980 is an order of magnitude smaller than the seismically imaged reservoir. Consequently, we believe that the point-source deformation model is reasonable as a first approximation, and the resultant depth represents a point within the deep reservoir. We cannot rule out an alternative possibility that the point-source model is not appropriate due to shallow creep of the flanks of the volcano into the crater (Swanson, personal communicaton 1990); however, the coincidence of the point-source depth solutions to the estimates of magma reservoir depth from seismic and petrologic data leads us to favor the deep source model.

A shallow magma reservoir?

There is abundant evidence (Hoblitt et al. 1981; Moore and Albee 1981) that the lateral blast of 18 May 1980, and many of the phenomena that occurred during the preceding two months were caused by the intrusion of a 0.11-km^3 dacite cryptodome into the north side of the seventeenth–eighteenth century summit dome (Fig. 3). Numerous shallow (<3 km) earthquakes were pro-

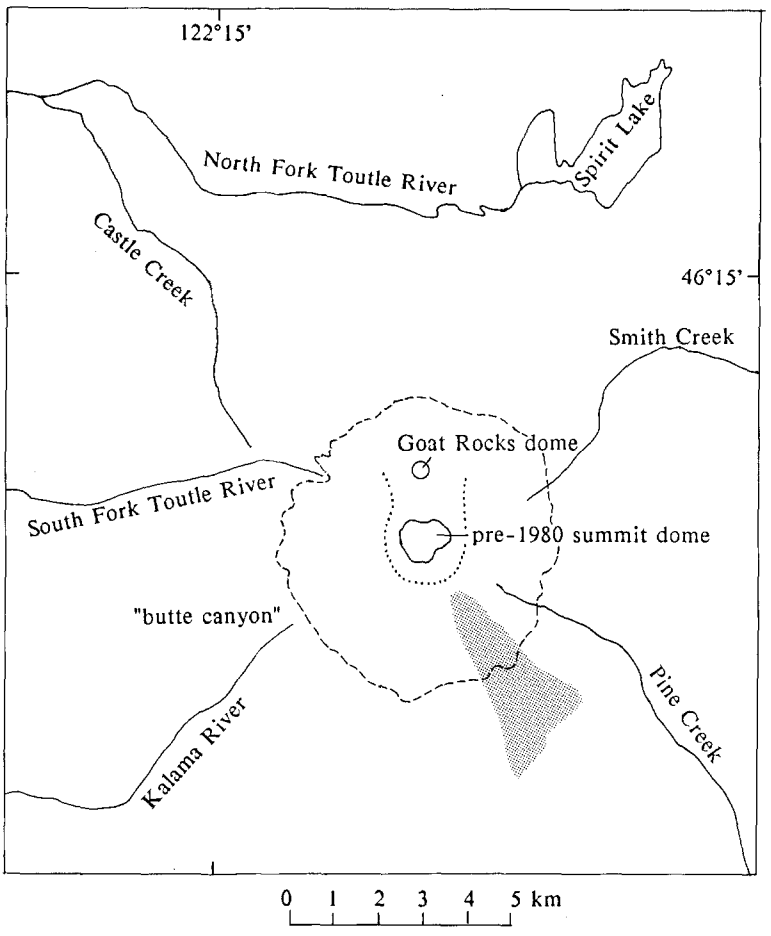

Fig. 3. Locality map of Mount St. Helens. Drainage is shown as it was before 18 May 1980. *Dashed line* is the 1500-m contour; *dotted line* is the rim of the crater formed in 1980; *shaded area* shows approximate extent of the 'worm complex' lava flows of Kalama age. The Goat Rocks and summit domes were destroyed by the avalanche and eruption of 18 May 1980

duced by fracturing of rocks as magma intruded the base of the volcano (Malone 1990). The cryptodome intrusion was destroyed by the morning eruptions of 18 May.

The debate regarding shallow magma reservoir(s) at Mount St. Helens does not directly concern the cryptodome; instead it centers on the possible existence of a shallow (<7 km) intrusion that may have been emplaced *below the level of the present crater floor,* either before or after 18 May. The principal argument for a shallow intrusion comes from mass balance of sulfur, based on data from gas emissions and glass inclusions (Casadevall et al. 1981, 1983; Gerlach and Casadevall 1986). Casadevall et al. (1983) argue that a relatively large volume of magma (containing $\sim 1.8\ km^3$ melt) was emplaced at shallow levels beginning several months before 18 May, and thereby escaped detection by all but the earliest (6 May–13 June; Dvorak et al. 1981) deformation monitoring. Of this volume, $0.11\ km^3$ intruded the cone to produce the cryptodome. Sulfur mass balance suggests that the 18 May eruption degassed about $1.4\ km^3$ of melt and the remaining $0.3\ km^3$ intruded to shallow levels and reached volatile saturation by early June 1980. According to this scenario, only about one third of the degassed magma was erupted; the remainder would reside at shallow levels, perhaps as a pressure-quenched stock within a few kilometers of the crater floor (TJ Casadevall, personal communication, 1990).

Although we cannot categorically rule out the possibility that a shallow intrusion was emplaced below the present crater floor during the spring of 1980, we do not find the evidence to be convincing. Uncertainty in the inferred concentration of sulfur in the pre-eruptive magma, as well as lack of edifice-wide deformation and intrusion-related seismicity (see below), cast doubt on the shallow magma reservoir model. The sulfur mass balance assumes that microprobe analyses of glass inclusions (with about 100 ppm sulfur, Sigurdsson 1982; cf. Devine et al. 1984) are representative of unexsolved Mount St. Helens dacite. However, 100 ppm sulfur is considered low for an undegassed dacitic magma (TH Gerlach, personal communication 1990); it is theoretically possible for much greater amounts of sulfur to be dissolved in dacitic melts. 18 May dacite melt at 920° C and $\log f_{O_2} = -10$ (Rutherford and Devine 1988) would be sulfur-saturated at about 800 ppm, based on experimental data for anhydrite stability (Carroll and Rutherford 1987). Presence of high sulfur abundances (to 870 ppm) in dacite glass inclusions within hornblende (and lower abundances within other phenocrysts) from Redoubt volcano suggests that sulfur is exsolved to a fluid phase prior to trapping of most melt inclusions in intermediate to silicic magmas (Gerlach et al. 1990). We suggest that a large fraction of the observed sulfur emissions at Mount St. Helens may also be attributed to a separate fluid phase.

Shallow earthquakes (1–2 km) that accompanied the 1980 eruptions correspond to a zone of magma vesiculation and disruption; no evidence for a shallow magma reservoir of 'any significant size' (after 18 May 1980) was found by Scandone and Malone (1985). Similarly, lack of edifice-wide deformation was cited by Chadwick et al. (1983) as evidence that no magma bodies were emplaced within a few kilometers of the surface between late 1980 and the end of 1982. We believe that intrusion of a 1.8 km^3 magma body at shallow depth would have been detected by seismicity and visible deformation of the volcano (exclusive of the north-flank bulge). We are skeptical that the tilt data from the single Ape Cave North site (Dvorak et al. 1981) are regionally meaningful. The inflation pattern at this site was not recorded at the nearby Ape Canyon tilt station (Dvorak et al. 1981) and deformation outside the area of the north-flank bulge was not detected by geodetic leveling (Lipman et al. 1981a). We suggest that the large magma volume indicated by sulfur mass balance need not have been shallow and that the upper part of a deep (>7 km) reservoir was open, with respect to volatile transport, through a narrow (average 30–60 m radius) conduit to the surface, both during and following the 18 May eruptions. This explanation is favored by most of the seismic, petrologic, and subsidence data, which call on rapid transport of magma from ≥ 7 km depth on 18 May. It is also implicit in the fluid-transport model proposed by Weaver et al. (1983) for the explosive eruption of 19 March 1982 (UTC date 3/20/82).

The conduit and lava dome

Several workers consider the conduit at depths of less than 5 km to be the source of repeated additions of lava to the present dome between 1981 and 1986 (Chadwick et al. 1983, 1988; Endo et al. 1987; Criswell 1989). Crystal-size distributions in 1980 blast dacite and subsequent dome dacite suggest that continuous crystallization may have provided, through repeated volatile saturation of interstitial melt, the 'overpressurization' needed to drive the intermittent dome-building episodes from 1980 to 1986 (Cashman 1988). Phenocryst growth began at depth at least 30 years before extrusion, according to U-Th decay series data (Bennett et al. 1982), but microlite nucleation began when dacite magma intruded the cone during the spring of 1980 (Cashman 1988).

Chadwick et al. (1988) explained deformation preceding the 1981 and 1982 dome-building eruptions by using a model in which a shallow reservoir of 'eruptible' magma, whose top is at a depth of 2–3 km below the crater floor (Fig. 2), is connected to the dome by a narrow (12.5–50 m radius) conduit filled with degassed magma; the reservoir and conduit are separated by a 'pressure valve'. They suggested that the reservoir may just be a wide part of the conduit. When pressure increases in the model reservoir, possibly due to groundmass crystallization and consequent volatile saturation (Cashman 1988), the reservoir magma expands, moves upward, and pushes the degassed conduit magma ahead of it. The conduit magma then begins to intrude and deform the dome. The intrusion initially is slow and accompanied by low seismicity. Ascent rates increase over a period of 3–4 weeks as the degassed conduit magma is replaced by reservoir magma. After the degassed magma is expelled, the ascent rate increases sharply, causing increased dome deformation and shallow seismicity. The shallow reservoir magma then erupts quickly, probably within a few hours (Endo et al. 1987).

From hypocenters recorded from November 1988 to May 1989, Endo et al. (1990) documented two zones of seismicity: a deep zone at >4.5 km below the crater floor and a shallow zone at about 1.5–3 km (Fig. 2). The relatively aseismic zone between 4.5 and 3 km is interpreted as the lower part of a magma reservoir whose top is at about 1.5 km. Given a cylindrical reservoir with volume equal to that of the average dome-building eruption (3.7×10^6 m^3; Swanson and Holcomb 1990), Endo et al. suggested that the lower (4.5–3 km) 'reservoir' has a radius of 20 m. Following Chadwick et al. (1988), Endo et al. assumed that the conduit connecting the shallow magma reservoir to the dome has a radius of about 15 m. Between eruptions, a deeper reservoir whose top is at about 7 km was thought to replenish the shallow reservoir through a conduit of unknown dimensions. We regard the 'reservoirs' inferred by Chadwick, Endo, and coworkers as simply different regions of a narrow conduit that is plugged in its upper part. We believe the shallow magma 'reservoirs' that have been the source for most magma extruded during the 1980–1986 dome-building eruptions are the upper parts of the conduit system that extends downward to a larger reservoir at about 7 km depth. Modeled radii for the shallow 'reservoirs' (e.g. Chadwick et al. 1988; Endo et al. 1990) are less than (or at the low end of) the range of average conduit radii (30–60 m) inferred for the entire conduit (to ~ 7 km depth) on the basis of data from the 18 May eruption.

We realize that the conduit system probably has a more irregular geometry than shown in the cylindrical model (Fig. 2) and has evolved since 1980; the cylindrical model offers only a useful first approximation. Our observations of deeply eroded volcanic and plutonic terranes lead us to question whether isolated conduits with 'soda-straw-like' dimensions (Fig. 2) exist (or persist) in nature. Composite and radial dike swarms are common in eroded stratovolcanoes, and central regions are typically intruded to shallow levels by kilometer-diameter stocks (e.g. Sillitoe 1973). Many volcanoes are aligned and are believed to be fed from necks that emanate from dikes. In contrast, narrow cylindrical conduits are rarely recognized in the geologic record, probably due to a combination of the following factors: (1) narrrow conduits are unlikely to be preserved over large paleovertical distances; (2) upward stoping would tend to erase the deep roots of conduits; and (3) many conduits may actually be magma withdrawal pipes within larger intrusive masses (dikes or stocks).

With regard to possible dike emplacement models, there is seismic first-motion evidence to support a regional fault structure in the basement below Mount St. Helens (Weaver et al. 1981; Weaver et al. 1987). However, the hypocenter distribution for earthquakes that followed the large eruptions of May and June 1980, shows only limited lateral elongation of the 7- to 12-km-deep earthquake-free zone (Fig. 2). This observation is supported by focal mechanism solutions for the earthquakes, which indicate inward-directed stress (pressure differentials of 150 to 220 bars) produced by magma withdrawal from the 0.65- to 0.75-km radius earthquake-free zone at 7 to 12 km depth (Barker and Malone in press). At deeper levels (12 to 22 km), however, there is evidence of a dike-like feeder.

We believe that initial transport of magma through the crust below Mount St. Helens was probably accomplished by dike propagation. However, the preponderance of eruptions with central-vent sources through at least the late history of the volcano (Spirit Lake stage) indicate that once a feeder to the surface was established, magma transport became restricted to a cylindrical region below the principal vent. This inferred progression is consistent with fluid dynamic predictions in which stagnant parts of dikes crystallize, and flow becomes restricted to regions of propagation and magma delivery to the surface (Delaney et al. 1986). We tend to favor the interpretation of Nakamura (1977) that at polygenetic volcanoes 'repeated eruptions from the same vent may form a cone around the vent as well as a pipe-shaped vertical conduit which is stable enough to be continually used as the channelway for the ascending magma'.

It is likely that magma has been present continuously in the deep reservoir system at Mount St. Helens at least since the Goat Rocks eruptive period (see below). Ascent of magma to feed the cryptodome during the spring of 1980 must have followed the same general pathway as previous central-vent eruptions at Mount St. Helens. Ascent through shallow and brittle levels of the crust above the magma reservoir may have initially been by dike propagation, but once the eruptions of 18 May began, magma transport became restricted to a region below the vent that is best modeled as a cylindrical magma-withdrawal pipe. The conduit between the surface and 7 km is accordingly viewed as a magma-withdrawal pipe in Fig. 2, without regard to whether it is located within a larger dike or stock-like intrusive complex at depth.

Amphibole reaction rims: implications for conduit models

Magma ascent rates at Mount St. Helens have recently been assessed by comparing textures and widths of dehydration reaction rims on amphibole phenocrysts with those produced experimentally (Hill and Rutherford 1989; Rutherford 1990). Samples of 18 May 1980 pumice containing pristine amphibole were equilibrated at 920° C and 2 kb (water-saturated), then depressurized isothermally at various rates to a final pressure of 200–300 bars. Reaction rims 10–12 microns thick were produced in four-day runs. On the basis of these experiments, amphibole in magma that ascended rapidly on 18 May would not have had time, prior to quenching, to develop reaction rims. In contrast, samples of blast dacite from the cryptodome have mainly uniform 10- to 12-micron-thick rims, and 1980–1983 dome lavas have bimodal distributions of reaction rim widths with concentrations at 10–12 and 30 microns. For example, 31 October 1981 dome samples contain two sets of amphibole breakdown rims that average 10 and 45 microns in width, leading Hill and Rutherford to conclude that a portion of the magma moving into the dome had risen from about 7 km in four days. In a sample of October 1986 dome dacite, two-thirds of the amphibole crystals lack reaction rims, implying ascent of these crystals from depth in less than four days (Rutherford 1990).

Such interpretation of the reaction-rim data pose volume problems for the conduit models reviewed above. Although the amphibole-rim data suggest replenishment from 7 km, replenishing magma could not have displaced resident magma in the model conduit upward, because only about 0.002 km^3 of dacite was erupted during the four-day 31 October 1981 eruption (Swanson et al. 1987). Eruption of one to two orders of magnitude more magma would be required to displace all magma in a 30- to 60-m-radius conduit to a depth of 7 km. If the initial interpretations of the amphibole reaction-rim data are correct, magma ascent during the period of post-1980 dome growth must have been more complex than the single narrow-conduit models imply, possibly including a fivefold reduction in the average conduit radius (Rutherford 1990), or propagation of new feeders from the deep reservoir.

Alternatively, some of the amphiboles may be xenocrysts liberated from gabbroic inclusions during transport or upon eruption. Heliker (1984) pointed out that gabbroic inclusions in dome dacite are locally disaggregated and contribute xenocrysts to the dacite host. Our observations are in agreement; brown prismatically cleaved hornblende without reaction rims is a major component of some gabbroic nodules in the dome and would contribute euhedral to subhedral xenocrysts to the dacite host upon disaggregation. The presence of unreacted hornblende in the inclusions and xenocrystic clots having reaction boundaries only where hornblende is in direct contact with the dacite host demonstrate that the dehydration reaction is facilitated by the presence of melt at grain boundaries and that unreacted hornblende can be preserved during transport from depth within the gabbroic inclusions. Even reacted hornblendes within inclusions could liberate pristine cleavage fragments to the dacite host upon disaggregation. Liberation of unreacted amphiboles at various times during magma transport could also lead to multiple populations of reaction rim widths. The interpretation of ascent rates from reaction rim widths is therefore potentially complicated, although it may be possible to chemically or texturally fingerprint xenocrystic hornblende.

Mount St. Helens plutonic complex

The crust above 7 km probably contains solidified plutons or stocks related to previous eruptive periods at Mount St. Helens as well as Tertiary intrusions (e.g. Casadevall et al. 1983; Evarts et al. 1987; Lees and Crosson 1989). Abundant gabbronorite and diorite xenoliths in the post-1980 dome (Heliker 1984), in dacite pumice (Scarfe and Fujii 1987), and in domes, lava flows, and pyroclastic flows of the Pine Creek, Castle Creek, Kalama, and Goat Rocks eruptive periods (Fig. 1) (Pallister et al. in press) are evidence for a composite plutonic complex below the volcano. Cumulus textures, trapped melt, and oscillatory zoning in these xenoliths probably record crystallization along margins of the Mount St. Helens magma reservoir. Late crystallization of amphibole in the xenoliths indicates progressive volatile enrichment of an originally volatile-poor mafic magma (Scarfe and Fujii 1987). Amphibole-bearing dacites similar to those erupted in 1980 and amphibole-bearing gabbronorite xenoliths have been common though the 40 000-year magmatic history of the volcano (Hopson and Melson 1980; Smith and Leeman 1982, 1987). Amphibole stability and the common 1980-type phase assemblage require equilibration with volatile-rich magma (Merzbacher and Eggler 1984; Rutherford and Devine 1988). Long term residence of fluid-rich magma at depth is, therefore, consistent with the eruptive history of Mount St. Helens.

Gravity modeling suggests a large (to 18 by 22 km) shallow intrusive complex below Mount St. Helens (Williams et al. 1987), but there is little other evidence to support such a large shallow body. Wallrocks adjacent to the conduit system at shallow levels (<2 km) are the volcanic rocks of the constructional cone; at deeper levels the conduit and deep magma reservoir may penetrate a relatively small composite pluton that represents crystallization products of earlier eruptive periods at Mount St. Helens. This inferred Mount St. Helens pluton is hosted in a thick section of Tertiary volcanic rocks that are intruded by subvolcanic to epizonal plutons (Evarts et al. 1987). Broadly analogous Tertiary diorite to granite plutons near Mount St. Helens (the Spirit Lake and Spud Mountain plutons) are modeled as small-diameter cylindrical bodies that extend to depths of ~9 km on the basis of seismic tomography (Lees and Crosson 1989). Regional seismic refraction data also indicate that the lateral dimensions of shallow intrusions in the Mount St. Helens area are small (Mooney and Weaver 1989). Magnetotelluric data define a thick east-dipping conductor that is thought to represent compressed forearc basin sedimentary rocks in southern Washington; the top of this conductor is about 6 km below Mount St. Helens (Stanley et al. 1987). The conductor is not interrupted by rocks with different electrical properties, as would be anticipated if the region were underlain by a large plutonic complex.

The data summarized above and in the previous sections suggest that the Mount St. Helens magmatic system is fed from a deep (>7 km) and relatively large (5 to 7 km^3) reservoir (Fig. 2). Crystal-rich cumulus 'mush' likely forms ductile walls to the deep reservoir; such walls would be seismically imaged as part of the reservoir.

Crystallization, magma addition, mixing, and unloading may lead to overpressurization of the deep reservoir followed by intermittent magma transport through a relatively narrow conduit system to the surface. Magma in the upper part of the conduit system is relatively cool and degassed, and forms a plug whose viscosity increases with time. This plug may correspond to the upper 1.5 km of the conduit. During the period from late 1980 to 1986, vapor-saturation induced by groundmass (melt) crystallization in the shallow part of the conduit may have driven most of the small dome-building eruptions.

The deep magma body inferred from the earthquake-free zone at >7 km depth (Fig. 2) may be analogous to the concentrically zoned mafic plutons observed in deeply eroded arc complexes (Irvine 1967; James 1971; Snoke et al. 1982). It may also extend farther downward into a variably deformed mid- to lower-crustal layered mafic complex like that recognized below an uplifted arc terrane in northern Pakistan (Bard 1983), a zone in which dacites are generated by partial melting (Smith and Leeman 1987). Focal solutions for deep (12–22 km) earthquakes show preferential alignment with the regional stress field, and suggest that the deep root of the Mount St. Helens' magma system is a northeast-trending feeder dike within a tensional offset of the NNW-trending St. Helens seismic zone (Weaver et al. 1987; Barker and Malone in press).

Eruptive periods and chemical cycles of the past 500 years

Previous eruptive periods of Mount St. Helens provide models for forecasting the kinds of events that could occur in the future. Such forecasts are based on the assumption that future activity is more likely to resemble one or more kinds of past events than to initiate a wholly new eruptive style. For this reason we summarize eruptive activity that has occurred during the past 500 years, including the Kalama, Goat Rocks, and current eruptive periods, which is the best-documented part of the volcano's history. We then forecast potentially hazardous events that could occur either if the behavior pattern of the last several years continues or if a large volume of magma again moves upward from a deep reservoir.

Kalama eruptive period and the fingerprint of magma mixing

The Kalama eruptive period was preceded by a dormant interval of 600–700 years, which ended in A.D. 1480 (Yamaguchi 1983) with a voluminous explosive eruption of 66–67% SiO_2 dacite tephra (2 km^3 DRE;

Carey et al. 1989). The resulting tephra layer, W*n*, is as much as 150 cm thick at a distance of 10 km (Mullineaux 1986), 10 cm at 100 km, and 3 cm at 200 km from the volcano. Two additional tephra eruptions of much smaller volume ensued and were followed in A.D. 1482 by eruption of the W*e* tephra, with a DRE volume of 0.4 km^3 (Carey et al. 1989).

These early Kalama explosive eruptions were followed by the extrusion of one or more dacite domes near the summit (Hoblitt et al. 1980). Lithic pyroclastic flows caused by dome collapse and pumiceous pyroclastic flows resulting from explosive eruptions moved as far as 14 km down the Kalama River valley southwest of the volcano. These pyroclastic flows overlie the W*e* tephra and contain blocks of juvenile dacite with 64–67% SiO_2.

This early Kalama phase of dacitic volcanism, which continued for at least two years and perhaps as long as 25 years (Yamaguchi 1985; Hoblitt 1989), was followed abruptly by eruptions of andesite. The andesitic eruptions initially produced four tephra layers of set X. Scoria fragments from the set X tephra have 57–59% SiO_2. Three of the four layers are 4–12 cm thick at distances of 8–10 km northeastward and eastward from the volcano (Mullineaux 1986). Although the tephra layers are thickest in these directions, small amounts of the tephra also are present on other sides of the volcano, which suggests eruptions during changing wind directions, perhaps over a period of days to years.

The early andesitic tephra eruptions of Kalama time were followed by the extrusion of andesite lavas (57–59% SiO_2), which flowed as much as 6 km down most sides of the volcano (Hoblitt 1989). Their wide distribution suggests that the flows were extruded from a summit vent. Associated andesitic pyroclastic flows (also 57–59% SiO_2) moved as much as 8.5 km down the northwest and southwest sides of the volcano. Tree-ring analyses indicate that one of the pyroclastic-flow deposits was formed before A.D. 1570 (DK Yamaguchi, unpublished data).

The andesitic eruptions were followed by the extrusion of a summit dacite dome, perhaps starting during the first half of the seventeenth century (Hoblitt et al. 1980; Hoblitt 1989). Intermittent dome extrusion continued for nearly 150 years, accompanied by avalanches of hot dacite debris down most sides of the volcano, some of which triggered lahars by melting snow. The SiO_2 contents increased from 61 to 64% during this interval. Few avalanches, if any, reached more than a kilometer or two beyond the base of the volcano, but the lahars extended at least 10 km farther downvalley. In A.D. 1647 (Yamaguchi 1986), during dome extrusion, pumiceous dacitic pyroclastic flows descended the northwest side of the volcano. Paleomagnetic data indicate that summit dome extrusion continued until late in the eighteenth century (RP Hoblitt, unpublished data); thus, the Kalama period lasted about 300 years.

The eruptive products of the past 500 years (Kalama, Goat Rocks, and 1980 to present) have similar isotopic ratios and were probably all derived from the same magma reservoir (Halliday et al. 1983). Given a deep and relatively large magma reservoir similar to the 1980 magma chamber, the short time span of the Kalama period (~300 years) relative to conductive cooling times for large bodies of magma (e.g. Jaeger 1957) suggests only limited deep crystallization. For this reason and because of the relations described below, we believe that the wide range of rock compositions reflect mainly physical processes of magma mixing.

Petrographic and geochemical features indicate magma mixing and mingling during Kalama time. Banded pumice and scoria clasts occur in the W and X tephra sets; those in the dacitic W set contain olivine and augite xenocrysts. Banded scoria from the basal X tephra contains basaltic bands with olivine and 58% SiO_2 glass in an andesitic matrix with 66% SiO_2 glass. Phenocrysts in the W and X tephra sets show sieve textures and evidence of resorption. Kalama dacites are depleted in incompatible elements relative to associated basalts and andesites, precluding an origin solely by crystal fractionation of the mafic magmas (Smith 1984; Pallister and Hoblitt 1985; Smith and Leeman 1987). This relation and trace-element modeling of potential sources suggest that partial melting of mafic rocks played a role in the genesis of the dacitic magmas (Smith and Leeman 1987).

Rare earth element (REE) abundances for Kalama rocks decrease with increasing SiO_2 (Fig. 4), a relation that is contrary to the effect expected from removal of major phenocryst phases during fractionation. Although accessory-phase fractionation can produce decreasing REE with increasing SiO_2, the relatively uniform decrease in the REE by a factor of about 1/2 with little change in pattern slope, the petrographic evidence for mixing, and the variation of other major and trace elements (described below) are more readily explained by mixing of Kalama dacite with REE-enriched basalt

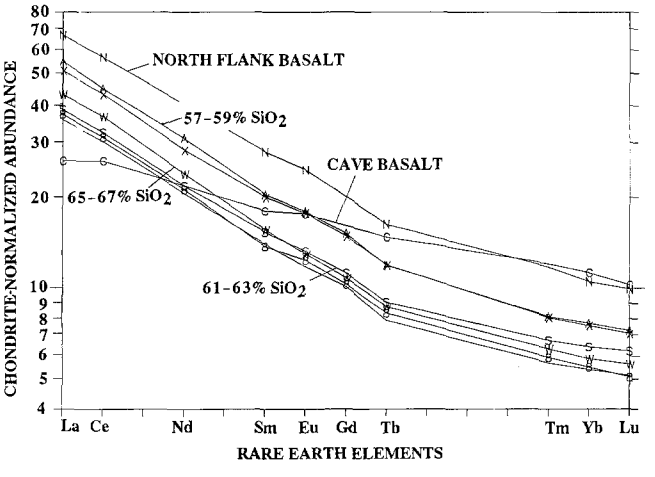

Fig. 4. Chondrite-normalized rare-earth element abundances. Symbols: *A*, andesite lava (worm complex and related flows); *X*, scoria from set X tephra; *W*, pumice from set W tephra and overlying pyroclastic flows; *S*, Summit Dome dacite; *8*, 1980–1986 dacite; *C*, cave basalt; *N*, north flank basalt. *Unlabeled* line at lowest abundance; dark scoria from 6 January 1990 eruption. Each pattern represents average of two to ten individual analyses. SiO_2 ranges given for Kalama age rocks (see Fig. 7). Sources: Pallister and Hoblitt (unpublished), basalts from Smith (1984)

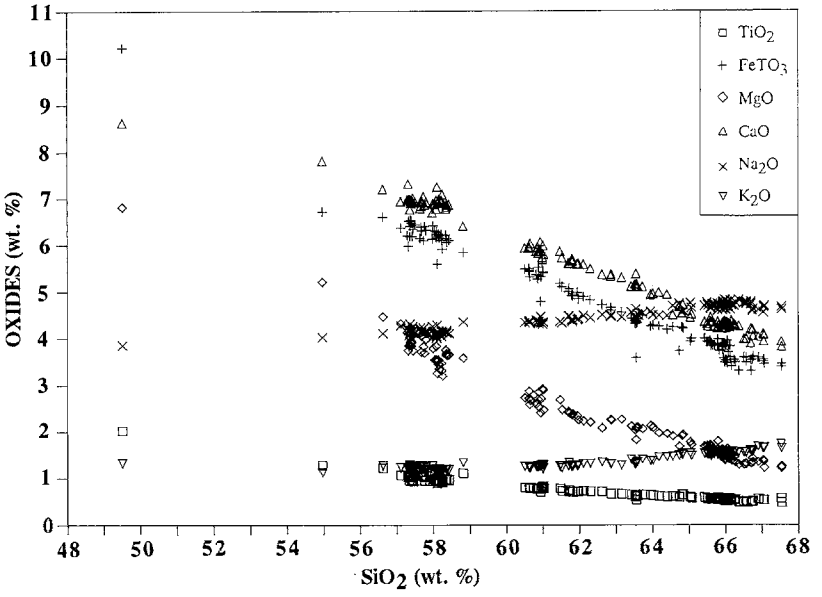

Fig. 5. SiO_2 variation diagrams for rocks of the Kalama eruptive period and for north-flank basalt of Smith (1984). $FeTO_3$ = all Fe given as Fe_2O_3

similar to that erupted during the preceeding Castle Creek period (Fig. 1). Two geochemical distinct basalt types were erupted: the 'cave' and 'north flank' types of Smith (1984). The north-flank basalt was erupted from the summit area of the volcano near the end of Castle Creek time. North-flank basalts have REE patterns that are parallel to those of the Kalama andesites and dacites, but at *higher* abundance levels. In contrast, the cave basalt has a crossing pattern and, therefore, cannot be directly linked to petrogenesis of the Kalama dacites (Fig. 4).

Analytical data for Kalama rocks define single linear trends on SiO_2-variation diagrams for most major elements and for the trace elements Sr, Y, Sc, Co, V, U, and Th, relations that suggest two-component magma mixing. The linear major-element trends either intersect or approach values in north-flank basalt at ~49% SiO_2 (Fig. 5). In contrast, data for the high field strength elements (HFSE, ionic charge/radius <0.25; Nb, Ta, P, Zr, Ti), as well as for Cr and the REE, reveal a more complex chemical evolution for the Kalama rocks. These data produce multiple trends on SiO_2-variation diagrams (Figs. 6 and 7). The trends form 'counterclockwise loops' with respect to stratigraphic position: Ta increases as SiO_2 decreases during the early part of the Kalama period (A. D. 1480–1505), then decreases at near-constant SiO_2 in middle Kalama andesite lavas and decreases with increasing SiO_2 in the late Kalama summit dome samples (Fig. 6). Data for the lithophile elements K, Rb, Li, and Ba also form SiO_2-variation loops with respect to stratigraphic position, but these trends are not as well defined as those for the HFSE and Cr. In the discussion that follows, we use the SiO_2–Cr diagram (Fig. 7) for illustrating details and for comparison with data from later eruptive periods because the trends are especially well-defined and are representative of the HFSE trends. Our instrumental neutron activation analyses (INAA) for Cr typically have coefficients of variation of <3%, and we have replicated the trends using rock fragments analyzed at different times. First, we deal with the early part of the Kalama loop.

The early Kalama trend of increasing Cr (and HFSE) with decreasing SiO_2 (W-tephra through X-tephra, Fig. 7) may be explained by addition of basalt similar to the north-flank type to W-pumice magma. Least-squares modeling, using the approach of Wright and Doherty (1970), shows that the major-element composition of set X scoria fragments can be produced by mixing subequal proportions of W-pumice and north-flank basalt. Abundances of the REE (Fig. 8), as well as Cr and the HFSE, calculated using proportions from the least-squares solutions, are in excellent agreement with actual abundances in the set X scoria. However, the model does not account for variation of the lithophile elements Rb, Ba, Th, K, and Sr, as abundances of these elements in the X-scoria are not intermediate between W-pumice and the north-flank basalts (Fig. 9). We do not believe this discrepancy invalidates the mixing hypothesis. The basaltic endmember may have been similar, but not identical, to the north-flank basalt used in the model calculations. North-flank basalts are somewhat variable in composition (note the difference in potassium contents of the two samples shown in Fig. 9). In addition, another component (a fluid phase?) may have affected the distribution of the elements in question. Although the discrepancy remains problematic, agreement of the major elements and most other trace elements with the mixing model, as well as petrographic evidence of mixing, leads us to conclude that the early part of the Kalama (A. D. 1480–1505) was dominated by relatively simple two-component magma mixing of dacite with basalt similar to the north-flank type.

The unusual depletion of incompatible trace elements in Mount St. Helens dacite (Smith and Leeman 1987) is evident in Fig. 9. The north-flank basalt has the trace-element signature of a within-plate or ocean-island basalt (OIB) and lacks the HFSE depletions that

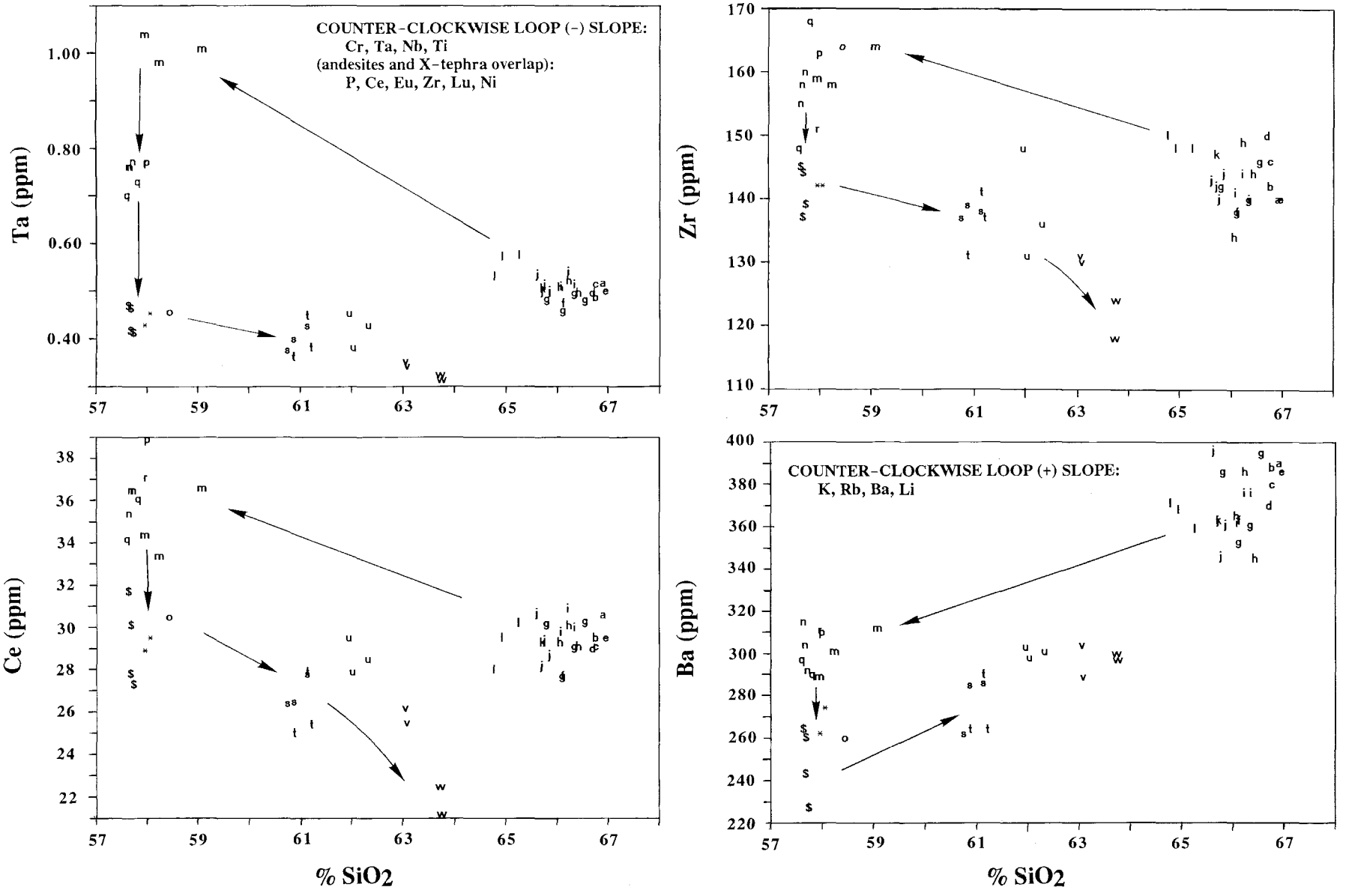

Fig. 6. SiO_2 variation diagrams showing trace element data from rocks of the Kalama period. *Arrows* indicate stratigraphic sequences and define counter-clockwise loops with either negative slopes or positive slopes; elements are indicated for which similar loop patterns are seen. Symbols: *a–f*, W-tephra pumice; *g–l*, pumice from early Kalama pyroclastic flows; *m*, scoria from X-tephra; *n–q*, *, $, andesites (mainly worm complex lavas); *s–w*, summit dome (prismatically jointed blocks, pumice, and blocks emplaced above paleomagnetic blocking temperatures). Precision, expressed as standard deviation of multiple analyses is 3%–6% at the abundance levels shown. Ta, Ce, and Ba analyzed by INAA, Zr by energy-dispersive XRF

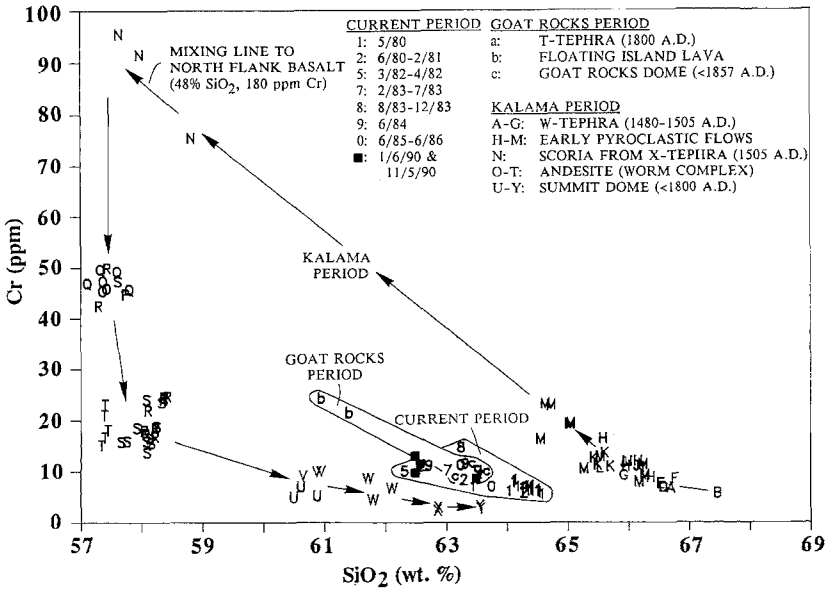

Fig. 7. SiO_2–Cr variation diagram for samples from the Kalama, Goat Rocks, and current eruptive periods at Mount St. Helens. Analyses of SiO_2 and Cr were by XRF and INAA, respectively, in USGS Denver laboratories. Current period samples with $<62\%$ SiO_2 are not shown because INAA Cr data are not available. SiO_2 was corrected to a volatile-free, 100% major-element basis after all iron was assigned to Fe_2O_3. All tephra samples are of pumice or scoria; pyroclastic-flow samples include prismatically jointed blocks or blocks determined to have been emplaced above paleomagnetic blocking temperatures. Age progession is indicated by alphabetical and numerical squences and vectors (Hoblitt 1989; Swanson et al. 1987; Swanson and Holcomb 1990; Yamaguchi 1983, 1985; Yamaguchi et al. 1990). *Filled squares* indicate composition of dark scoria in 6 January and 5 November 1990 tephra

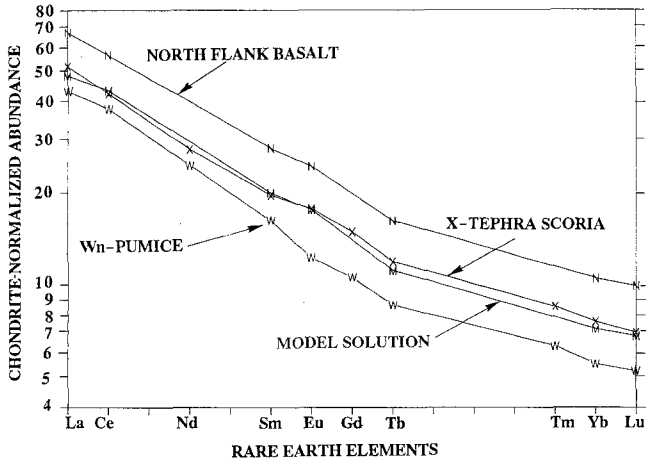

Fig. 8. Chondrite-normalized rare-earth element abundances for north-flank basalt (*N*), pumice from set W tephra (*W*), scoria from set X tephra (*X*), and mass-balance model solution (*M*), in which M = 49% W + 42% N + 7% plagioclase + 1% olivine. Model proportions based on major-element least squares solutions in which compositions of olivine and plagioclase are those in north-flank basalt. Similar pattern results from least-squares solution for mixture of 51% N + 49% W. See Fig. 4 for data sources

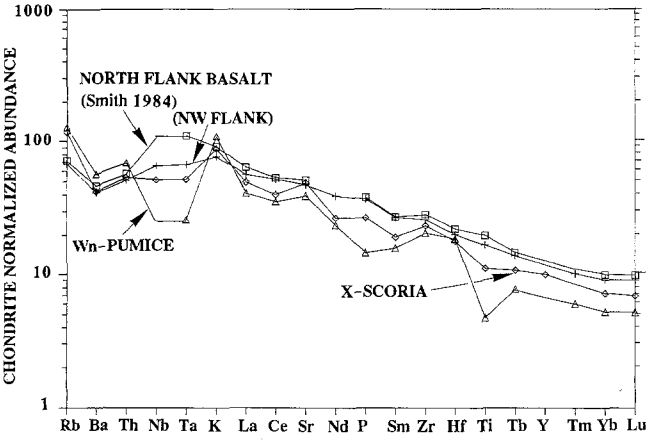

Fig. 9. Extended chondrite-normalized trace-element diagram ('spidergram', Thompson et al. 1983) showing patterns for pumice from the W*n* tephra, scoria from the X tephra, average of four north-flank basalt samples from Smith (1984), and representative sample from a section of several north-flank basalt flows at the head of Studebaker Creek, on the northwest flank of Mount St. Helens. Absence of symbol for Nb indicates lack of data (north-flank basalt) or below detection limit (W*n* pumice); lines are extrapolated assuming chondrite normalized abundances of Nb are equivalent to those for Ta in these samples

characterize most calc-alkalic arc basalts (Fig. 9; cf. Pearce 1982; Leeman et al. 1990). The elemental abundances that are most different between the Kalama dacites (such as W*n* pumice) and the north-flank basalt are the HFSE and Cr. Consequently, they offer the best chemical fingerprints of mixing of north-flank-type basalt with the dacites. These are the same elements that best display 'loop' patterns on SiO_2-variation diagrams.

The HFSE-enriched fingerprint of OIB dies out during the remainder of the Kalama period, dropping abruptly during the middle-Kalama andesitic interval, then more gradually during growth of the summit dome. The andesite lavas and pyroclastic flows, which were erupted after tephra set X, may also be products of magma mixing; but their lower (and bimodal) Cr and HFSE abundances at equivalent SiO_2 (Fig. 7) are more difficult to model and probably require additional, poorly constrained, magma-mixing endmembers. At first inspection, fractionation of Cr- and HFSE-enriched spinels and other accessory minerals such as apatite and zircon appear to offer an alternative explanation for the decrease in HFSE abundance at near-constant silica and the resulting silica-variation loops. Though not impossible, there are problems with this alternative: (1) accessory-phase fractionation would have to take place with little or no accompanying silicate fractionation (major element compositions of the ande-

sites show little variation); and (2) similar loop patterns for the incompatible large-ion lithophile elements Rb, Ba, and K are not readily explained by fractionation of common accessory phases.

Basalts of the OIB geochemical type are unusually abundant in the southern Washington Cascades compared to other calc-alkalics arcs, a feature that led Leeman et al. (1990) to suggest a relatively minor flux of subducted sediments and dehydration fluids at Cascade magma sources due to the youth of the subducted slab. This situation not only allows one to 'discern more clearly the effects of processes operating in the mantle wedge' (Leeman et al. 1990), but it also allows us to more clearly discern mixing of this distinctive basalt type at individual Cascade volcanoes.

Following eruption of the andesites, the dacite summit dome marked a return to high-SiO_2 compositions near the end of the Kalama period (Hoblitt et al. 1980). Hopson and Melson (1984, 1990) suggested that the return to a high-SiO_2 magma was the result of the delayed rise of a dacite plug, which had been generated early in the Kalama period. However, the summit-dome dacites are geochemically distinct. They have lower SiO_2, P, Ti, Cr, Ni, Ta, Nb, and Zr than the early Kalama dacites, and they show a stratigraphic progression from 61% to 64% SiO_2, a trend that is opposite in sense to that of the early Kalama dacites (67% to 65% SiO_2) (Fig. 7). These chemical data, the stratigraphic sequence, and the dendrochronology age of A. D. 1647 for a pumiceous summit-dome dacite pyroclastic flow (Yamaguchi 1986), lead us to conclude that the stratigraphic sequence dacite-andesite-dacite of the Kalama is also the magmatic sequence.

Goat Rocks eruptive period

The next eruptive period began in A.D. 1800 when an explosive eruption resulted in the deposition of the dacite tephra layer T, which extends northeastward from the volcano. The tephra has a DRE volume of 0.5 km^3 (Carey et al. 1989) and is about 50 cm thick at a distance of 10 km and 2 cm thick at 100 km. Although little time passed between the end of the Kalama period and the beginning of the Goat Rocks period (Fig. 1), the eruption of the T tephra marks the beginning of a new chemical cycle, characterized by slightly higher Cr than late Kalama summit dome dacite and by a reversal in the SiO_2 trend (Fig. 7). Eruption of the T-tephra was followed within a few months (Yamaguchi et al. 1990) by the extrusion of a 5-km-long, high-silica andesite lava flow on the northwest side of the volcano (the 'floating island' lava flow). Eruptive activity ended with the extrusion of the Goat Rocks dacite dome, which was completed by 1857. Pyroclastic flows caused by avalanches of hot rock debris from the north side of the growing dome descended to the north base of the volcano, and mixing of this debris with snow generated many small lahars.

The chemical sequence in Goat Rocks time from dacite to high-silica andesite, then back to dacite, forms a linear trend on the SiO_2–Cr variation diagram that is distinct from the trends of Kalama rocks (Fig. 7). This trend projects toward the high-Cr 'worm complex' lavas at 57–58% SiO_2 at one end and dacite from the 1980 blast deposit at 64.5% SiO_2 at the other.

Current eruptive period

The events that initiated the current eruptive period are well documented in U.S. Geological Survey Professional Paper 1250 (Lipman and Mullineaux 1981), which includes an account by Christiansen and Peterson (1981) on which the following summary is based. An earthquake swarm that began in late March 1980, was followed by a crater-forming steam explosion on 27 March, and similar explosions continued intermittently into mid-May. During this period, the 0.11 km^3 cryptodome was emplaced into the north flank of the volcano. On 18 May, a magnitude 5+ earthquake triggered a massive landslide on the north flank of the volcano, unloading the magmatic system, and generating a lateral blast followed by a paroxysmal eruption. The lateral blast devastated a 600-km^2 area north of the volcano and was immediately followed by a Plinian eruption column that rose to a height of >20 km. Tephra produced by this explosive eruption was carried downwind for more than 1500 km east of Mount St. Helens, and pumiceous pyroclastic flows extended to the north base of the volcano. Lahars and floods were generated by the rapid melting of snow and ice, and from water derived from the landslide deposits. Smaller eruptions on 25 May, 12 June, 22 July, 7 August, and 16–18 October each produced pyroclastic flows and eruption columns more than 10 km high, which resulted in deposition of tephra in various downwind directions. Extrusions of dacite in the crater in June and August built domes that were destroyed during explosive eruptions, but a dome that appeared during the October eruption continued to grow during at least 15 eruptive episodes between 1981 and October 1986 (Swanson et al. 1987; Swanson and Holcomb 1990). The period from late 1986 until the time of this writing (1990–1991) has been relatively quiet, although small gas-release explosions and changes in seismicity (described below) have taken place.

Chemical compositions from the current eruptive period, like those of the Goat Rocks and Kalama periods, show an overall trend of decreasing, then increasing SiO_2 contents (Cashman and Taggart 1983; Fig. 1 of Cashman 1988; Swanson and Holcomb 1990). In contrast to the earlier periods, a wide range in SiO_2 has also been discriminated in the detailed stratigraphic record of the initial eruptions. The 18 May 1980 eruptions produced mostly chemically homogeneous dacite with an average SiO_2 content of 64–65%. However, late in the day, SiO_2 contents ranged from nearly 65% to as low as 60.6% (Criswell 1989). Samples of rocks erupted after 18 May define a longer-term trend of decreasing SiO_2, from a high of about 64.5% in late May 1980, to a low of 61–62% by mid-1981, then recovering to 63–

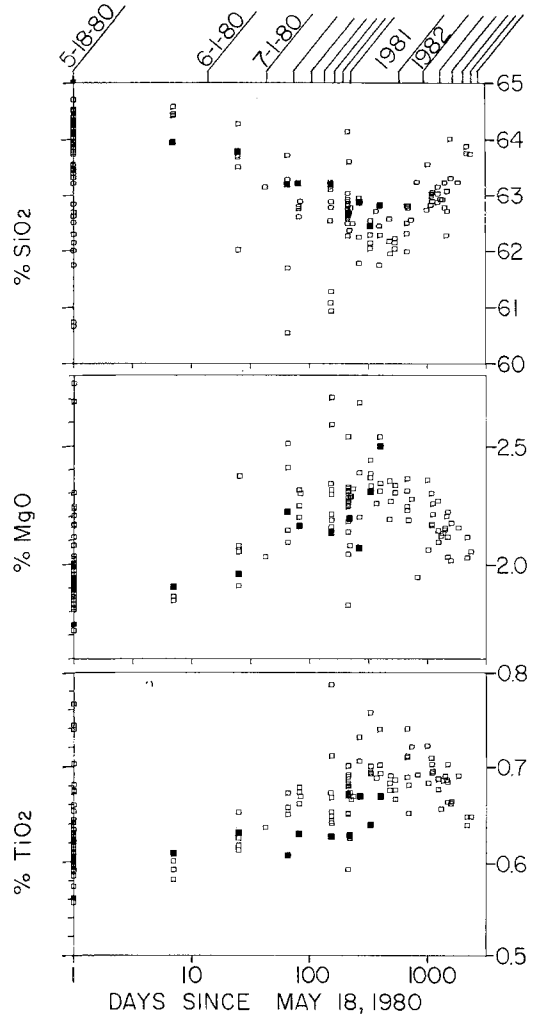

Fig. 10. Variation in SiO_2, MgO_2, and TiO_2 in eruptive products of Mount St. Helens for the period 1980 through 1986. Data from USGS archives (136 analyses), from Criswell (1987) (24 analyses of 18 May 1980 pumice), and averages of analyses from Bennett et al. (1982) (*filled squares*). Oxide abundances are recalculated on a volatile-free basis with all iron expressed as Fe_2O_3

63.5% by 1983. K_2O and Na_2O show parallel trends and are positively correlated with SiO_2 abundance, whereas CaO, MgO, TiO_2, P_2O_5 and total iron are negatively correlated with SiO_2. With time plotted on a logarithmic scale, the protracted trend of decreasing, then increasing, SiO_2 is especially clear (Fig. 10).

Products of the current eruptive period lie along a SiO_2–Cr trend similar to that of the Goat Rocks period (Fig. 7). As in early Kalama time, there is only indirect evidence for the presence of basalt in the magma reservoir during this period. Gabbroic inclusions (some with trapped melt) are common (3–4%) in the 1980–1986 dome rocks (Heliker 1984). Basaltic whole-rock compositions of noncumulus nodules, relatively high-Mg olivine (to Fo_{77}) and clinopyroxene (Mg# to 85), and calcic plagioclase (to An_{81}) led Heliker to conclude that the inclusions are not just crystal accumulations from the current period dacite, but instead represent crystallization of basaltic magma at depth. The current eruptive period therefore tapped or traversed a region that had recently contained mafic magma. However, the SiO_2 content of most volcanic rocks erupted during the current period decreased only to a low of about 61–62%. In this respect, products of the Goat Rocks and current periods represent two diminishing oscillations following the major perturbation of the magmatic system brought about by influx of basaltic magma during the Castle Creek and Kalama periods.

Post-1986 events and explosions of 6 January and 5 November 1990

There has been a remarkable change in seismicity since 1987. The seismically quiet zone of 1981–1986 at about 3–7 km depth has become the locus for hundreds of small earthquakes, suggesting that 'Mount St. Helens is not through with the current eruptive period and stresses are currently increasing in the top of the magma chamber and conduit' (Malone 1990). The newly activated region of seismicity suggests increased rigidity of the conduit at intermediate depths. This could result from contraction accompanying crystallization of the degassed conduit magma, or from directed stress (upward or downward) from the underlying magma reservoir acting on the largely crystallized conduit and resulting in plug creep. Hypocenter locations for the intermediate-depth (3–7 km) earthquakes appear to have a lateral distribution similar to that surrounding the deep (7–12 km) reservoir in 1980 (SD Malone, personal communication, 1990; Scandone and Malone 1985). Focal mechanism solutions for some of these earthquakes indicate strike-slip motion with principal stress axes at low angles ($<20°$) and at right angles to regional trends, relations that suggest a local volcanic source (Moran and Malone 1990). Consequently, upward stoping, new dike propagation, and possibly shouldering-aside of roof-rock blocks may have enlarged the lower part of the conduit (Fig. 2).

The eruptive hiatus that began in 1986 has been interrupted by small explosions, beginning in late 1989 and continuing sporadically into 1991. These explosions (or minor eruptions) occurred during a relatively quiet period of the post-1987 shallow-to-intermediate-depth seismicity. However, 2 h of emission-type tremor followed a magnitude 2.7 event at 0537 PST on 6 January 1990; hypocenters for this earthquake and for other smaller earthquakes that accompanied and followed the period of tremor were located less than 2 km below the dome (SD Malone, personal communication, 1990). A brief explosive episode at 0537 on 6 January ejected ballistic tephra and a small amount of ash, and triggered rock avalanches. The tephra was dominated by lithic fragments from the dome, but included minor ($<1\%$) dark scoria of Fe-Ti-oxide-bearing, augite-hypersthene-hornblende high-silica andesite. Most of the hornblendes have reaction rims about 30 microns thick. All contain brown glass as a groundmass phase, with varying proportions of microlites of feldspar and pyroxene. The microlites are smaller (commonly <0.02 mm in length) than in late dome samples (see

Table 1. Bulk rock and average matrix glass composition from dark scoria of 6 January 1990

	SiO_2	Al_2O_3	FeO[t]	MgO	CaO	K_2O	Na_2O	TiO_2	Sum
Bulk SH-208	62.6	17.6	4.91	2.50	5.51	1.29	4.60	0.68	99.93
Bulk SH-209	62.5	18.2	4.56	2.21	5.31	1.31	4.61	0.69	99.59
Matrix Glass	77.6	11.6	1.50	0.18	0.76	3.20	4.53	0.38	99.74

Oxide abundances, wt%

[t] Total Fe as FeO

Sources: Matrix glass from sample 1-6-90 analyzed by JS Pallister and GP Meeker using an ARL-SEMQ microprobe with 20-micron-beam diameter and 10 nanoamp sample current. Microprobe analyses corrected for Na_2O loss (7% for the 20 s count Na_2O data) using iterative 4 s count data. Bulk samples analyzed by X-ray fluorescence by JE Taggart and DF Siems of USGS

Cashman 1988) and lack the devitrified groundmass of surface-cooled samples. Brown glass has been observed in other dome samples and is attributed to submicroscopic oxide grains (KV Cashman, personal communication, 1990).

Dark fragments were also a trace component in tephra produced by an explosion on 5 November 1990. These are also Fe-Ti oxide bearing, augite-hypersthene-hornblende high-silica andesite and low-silica dacite. In contrast to the samples examined from the 6 January tephra, one of the samples is nonvesicular and contains some hornblende phenocrysts that lack reaction rims and others with thin (~10 micron) rims.

The dark scoria from the 6 January eruption has a bulk-rock SiO_2 content of ~62.5% SiO_2, but the glassy matrix is a high-silica rhyolite (77.6% SiO_2) (Table 1). It clearly does not follow the trend toward higher SiO_2 with time in dome lavas (Fig. 10). It is chemically most like the low-silica dacites and silicic andesites erupted during late 1980 and 1981 (cf. Melson 1983). As with samples of matrix glasses from the dome, the high oxide totals indicate extensive degassing. The dark scoria is chemically distinct from Kalama period rocks; rather, it has Cr abundances (Fig. 7) and REE patterns (Fig. 4) that overlap with low-silica dacites of the current eruptive period. We believe the dark scoria represents either unusual quenched fragments of early (1981) phases of the composite dome or 1981-vintage magma that was stored in the shallow levels of the conduit, degassed and variably oxidized, but did not undergo extensive groundmass crystallization. It is not xenolithic material from the Kalama period as early reports suggested.

A fluid-dynamic model

In contrast to the magma-mixing-dominated model we propose for the Kalama period, we explain the high-low-high silica cycles of the short-duration Goat Rocks and current eruptive periods using fluid dynamic models of magma withdrawal (Fig. 11; Spera et al. 1986; Blake and Ivey 1986a, 1986b; Boden 1989). In our model, a cycle begins with eruption of dacite from the top of a zoned reservoir wherein dacite overlies more mafic magma of greater density but lower viscosity (Fig. 11a). As the eruption proceeds, mafic magma (high-silica andesite) is coned upward toward the conduit entrance and is entrained (Fig. 11b). The result is eruption of mingled high-and-low-silica magmas like those of the afternoon of 18 May 1980 (as noted by Criswell 1987) and the eruption ends as high-silica andesite invades the conduit (Fig. 11c). Following the eruption, dacite remaining near the roof of the chamber reestablishes a planar surface below the conduit entrance and again invades the conduit (cf. Boden 1989). Movement of dacite back into the conduit produces an inversion in conduit magmas; mafic magma overlies the invading dacite.

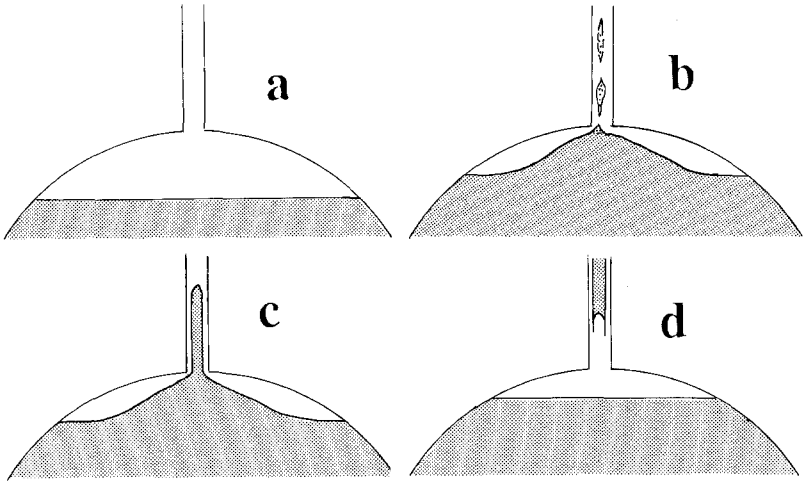

Fig. 11a–d. Cartoons showing the behavior of higher SiO_2 magma (*white*) and lower SiO_2 magma (*stippled*) during an eruptive episode at Mount St. Helens: **a** episode begins with a voluminous higher SiO_2 (dacite) eruption from top of a compositionally zoned magma chamber; **b** eruption causes magma interface to rise toward conduit; **c** as eruption continues, the interface enters the conduit and both magmas erupt; **d** as the eruption slows or stops, a planar surface is reestablished between the magmas in the reservoir. Lower SiO_2 magma trapped in the conduit is subsequently erupted intermittently as small-volume additions to a dome until the invading dacite arrives at the surface and the SiO_2 trend is reversed

During subsequent small eruptions, more dacite will move into the conduit and cause the interface to migrate upward; the migration may be accompanied by mixing of the invading dacite, the more mafic magma, and any residual primary dacite. On average, the SiO_2 content of erupted lava will decrease until the invading dacite first arrives at the surface; the SiO_2 content will then begin to increase. Progressive, rather than abrupt, changes in composition are explained either by gradational boundaries in a zoned source reservoir, or by mixing during transport in the conduit.

Carey et al. (1990) independently and concurrently developed a fluid dynamic model for the 18 May 1980 eruption that is similar to the one presented here. They use a model of magma withdrawal from a stratified reservoir to explain the eruption of silicic andesite during the most voluminous (pyroclastic flow dominated) phase of the eruption (1500–1630 PDT) followed by a decline in the amount of silicic andesite erupted during the final Plinian phase (1630–1700 PDT). Our models are in basic agreement; however, we believe the fluid dynamic model explains not only the eruption of silicic andesite on 18 May, but also the small-amplitude chemical cycle of 1980–1986 dome-forming eruptions.

The fluid-dynamic model provides a way to estimate the volume of the conduit. The model requires that the compositional inversion be implanted at the base of the conduit after a paroxysmal eruption as the compositional interface is reestablished in the deep magma reservoir (Fig. 11). Therefore, assuming pipe flow, the volume of material erupted after the paroxysmal eruption and before the compositional interface arrives at the surface should approximate the volume of the conduit. For the current eruptive episode, this includes material erupted from 25 May 1980, to the time the SiO_2 content began to increase, which was in October 1981 (Fig. 10). The aggregate volume of this material, compiled from Lipman et al. (1981b), Sarna-Wojcicki et al. (1981), and Swanson and Holcomb (1990) is about 0.06 km^3 DRE. If the conduit is assumed to be a circular cylinder with a length of 7 km, its radius must be about 50 m, in good agreement with the independent estimates of conduit radius discussed previously.

Future eruptive activity

We consider the above to be a working model; it may be revised or even discarded as new data become available. From the point of view of volcanic hazards assessment, details of the model are not critical because regardless of how they originated, cyclic chemical trends are apparent in the last three eruptive periods and are therefore pertinent to forecasts of future activity.

The current eruptive period has apparently completed a chemical cycle and, as noted by Gerlach and Casadevall (1986), magmatic volatile contents of gas emissions have declined. However, we cannot be sure that the current cycle is small-amplitude, such as that of the Goat Rocks period, and is therefore virtually complete or if it is the beginning of a new large-amplitude and protracted chemical cycle like that of the Kalama period, which probably would involve more mafic magmas (andesite or basalt) derived from the deep magma reservoir or below. We evaluate the hazards associated with these two alternatives below.

Some evidence favors interpretation of the current period as a small-amplitude cycle. Juvenile eruptive products of the current and Goat Rocks eruptive periods are of similar volume, but of much smaller volume than the W*n* tephra that initiated the Kalama period. The eruption of that tephra probably caused a greater perturbation of the deep magma reservoir than the current eruptive period, even taking into account the removal of lithostatic load by the landslide in 1980.

Small-amplitude cycle

Although no material has been added to the dome since October 1986, additional small-volume eruptions or explosions are still possible. Because of the length of time since the last dome-building eruption in October 1986, crystallization of the shallow conduit magma has probably formed a plug beneath the dome. The pressure necessary to overcome this blockage may exceed that of any eruption since 18 May 1980, and so a resumption of dome growth may initially be explosive. A similar conclusion was reached by Fink et al. (1990) on the basis of a more detailed analysis of endogenous and exogenous dome growth.

Assuming no new magma rises from the deep reservoir, we anticipate that most future shallow-source eruptions will be mainly gas-release explosions driven by penetration of groundwater into still hot dome and conduit rocks or by continued groundmass crystallization of conduit magma. We believe the occasional explosions that began in 1989 are of this type. They have not resulted in dome growth, yet they pose a significant hazard in the crater area because they apparently occur without warning; neither seismic nor deformation precursors have been identified (EW Wolfe, personal communications, 1990, 1991). At least six explosions have produced ash-rich plumes during the period between December 1989 and March 1991, and several of these events showered large (up to 2 m) ballistic fragments over regions of several km^2 north and east of the dome. The explosions were accompanied by relatively small pyroclastic flows and surges, as well as by rock and snow avalanches and dilute lahars.

The explosions create zones of hazard to human life. The probability of a small tephra-producing explosion taking place on a given day was 1–3% by early March 1991 (calculated on the basis of six ash-producing explosions since late December 1989, or four ash-producing explosions since early November 1990). The highest hazard is within the crater itself, where relatively large areas (several km^2) were affected by the products of previous explosions. This hazard decreases progressively with increasing distance on all the outer slopes of the volcano beyond the crater. In addition, a zone of avalanche, lahar, and flood hazards extends northward

from the crater to the North Fork Toutle River and to an unknown distance downstream.

If additional small-scale dome growth eruptions were to resume, people and property beyond the base of the volcano would not be threatened directly, but avalanches of hot debris from the dome onto snow could trigger floods or lahars in the North Fork Toutle River (Waitt et al. 1983; Mellors et al. 1988). Seismic and deformation monitoring permit these minor extrusive events to be anticipated (Swanson et al. 1983). If the current eruptive period is over, it may be followed by a dormant interval (except for occasional minor gas-release explosions) of several or many decades, such as the one that followed the Goat Rocks eruptive period.

Large-amplitude cycle

The 1980–1986 activity could have initiated a longer period of intermittent volcanism like that of Kalama time. Observations of seismicity accompanying the 1980 eruptions suggest that ascent of new dacite magma from depth will likely be accompanied by shallow seismicity and probably by deformation in the crater; these features may be used to forecast future eruptions. Slower aseismic ascent of magma, especially at deep to intermediate levels, remains a possibility, and may only be detected from deformation, gas-emission, gravity, and thermal data.

In this scenario, we anticipate the eruption of andesitic tephras and lavas during the next two decades, followed by a progressive return to higher-silica dacite lavas. Although we believe this scenario is less likely than the one presented above, we cannot rule out the possibility that the events of 1980 were accompanied by addition of mafic magma into the deep reservoir. Such an influx of new magma may, in fact, have been recorded by deep (12–20 km) earthquakes late on 18 May 1980 (Criswell 1989) and, as in Kalama time, could lead to eruption of more mafic magma.

If activity during the current eruptive period follows this scenario, sometime within the next few decades Mount St. Helens could erupt andesitic tephra, pyroclastic flows, and lava flows. The most serious hazard created by andesitic volcanism probably is that of lahars and floods created by the melting of snow by pyroclastic flows.

The next major eruptive period

Assuming that the current eruptive period represents a small-amplitude cycle similar to that of the Goat Rocks period and is now nearly over, we will now forecast the nature of the next major eruptive period. It is possible that the 1980–1986 eruptions depleted the upper part of the deep reservoir in low-density 'eruptible' magma. Melson (1983) argued that decreasing water contents in phenocryst melt inclusions erupted during the period 1980–1982 suggest that the volatile-rich 'cap' of the deep reservoir was erupted and the volatile content of magma in the deep reservoir has declined. Such a conclusion implicitly assumes that melt inclusions held in the conduit for extended periods at high temperatures and low pressure have not leaked.

Even if the volatile content of the reservoir magma has declined, we do not know the composition or volume relations of the remaining magma at depth, nor do we know the residence time that is necessary for that magma to once again become 'eruptible'. Previous repose intervals between eruptive periods have varied widely, but the one between Kalama and Goat Rocks time apparently was less than 30 years (Fig. 1). If a conservative approach to hazards assessment is taken, it should be assumed that a substantial quantity of low-density, volatile-rich, and potentially explosive magma is either available now or could become available in the near future.

The model we propose for the next major eruptive period includes initial explosive eruptions of dacitic tephra in volumes as great as that of the W*n* layer of Kalama age or the T layer of Goat Rocks time, followed by the extrusion of dacite or high-silica andesite to form a dome or lava flow, or both. An episode of andesitic volcanism, as in Kalama time, could follow and include the eruption of tephra, pyroclastic flows, and lava flows, or the eruptive period could end with the extrusion of a dacite dome. Pyroclastic flows and lahars could accompany almost any of this eruptive activity and would not be contained by the crater. Dome growth in the crater of Mount St. Helens could result in lithic pyroclastic flows moving down the North Fork Toutle River valley. If dome growth continues, it could eventually fill the crater and spill pyroclastic flows onto any flank of the volcano.

Lava flows that reach beyond the flanks of the volcano probably will be formed only during periods of andesitic or basaltic volcanism. Many andesite flows of Kalama age only reached the base of the volcano or 1–2 km farther. The single lava flow of Goat Rocks age extended nearly 5 km from its source vent, but less than 2 km beyond the base of the volcano.

Lahars and floods can originate in a variety of ways, including the eruption of hot fragmental debris onto snow fields and the avalanching of masses of wet rock debris. Spirit Lake could be a source of a flood or lahar in the North Fork Toutle River valley if the lake were to spill across and cut down through unconsolidated pyroclastic-flow and debris-avalanche deposits that dam it (Glicken et al. 1989). However, Spirit Lake now drains through a tunnel cut in bedrock, which normally ensures that the lake will not overtop the dam (Sager and Chambers 1986). Displacement of enough water to overtop the dam would require a large volume of material moving rapidly into the lake basin. Such an event is unlikely if the volcano continues to behave as it has since 1980, but could result from a lahar, debris avalanche, or pyroclastic flow of large volume. The effects of future lahars and floods in the North Fork Toutle River valley will be mitigated by a sediment-retention structure 35 km downvalley from the volcano (US Army Corps of Engineers 1986), built primarily to trap

sediment resulting from normal hydrologic conditions in the upstream drainage basin during the next 50 years.

Our proposed model includes the kinds of eruptive activity that we believe to be most likely in the foreseeable future; it does not, however, include some less likely events of other kinds or magnitudes that occurred in the past at Mount St. Helens, the relative likelihood of which can not yet be realistically assessed. One such event is the eruption of voluminous basalt lava flows like those that occurred near the end of the Castle Creek period. Another is an explosive eruption of considerably greater volume than any of those of the last 500 years. Such an eruption in Ape Canyon time (Fig. 1) produced a tephra layer that is at least four times thicker than layer W*n*, of Kalama age, at a distance of 100 km from the volcano (Crandell 1980, p. 73; Mullineaux 1986). Very large pumiceous pyroclastic flows and lahars resulted from this eruption or perhaps from other, similar eruptions in Ape Canyon time.

Hazard zonation

Areas threatened by future eruptions of Mount St. Helens have been portrayed on hazard-zonation maps published both before (Crandell 1976; Mullineaux 1976; Crandell and Mullineaux 1978) and after the 1980 eruptions. The general outlines of hazard zones at Mount St. Helens in late March 1980, are shown by Miller et al. (1981, Fig. 454), and an accompanying map (Fig. 455) shows hazard zones around the volcano as they were perceived in late May 1980. This map is still valid today. Newhall (1982) quantified intermediate- and long-term probabilities of volcanic hazards and translated these probabilities into estimates of risk to human life. Using these data, he compiled maps (scale about 1:250000) which portray the *annual* risk to human life from volcanic activity in areas around Mount St. Helens. His four maps show risk zones as of February 1980 (before precursory activity began), June 1980, August 1981, and February 1982.

Conclusions

Mount St. Helens is the most explosive and frequently active volcano in the western conterminous USA, and our previous hazards assessment of it (Crandell and Mullineaux 1978) is still generally valid. The eruptive period that began in 1980 greatly changed the shape of the pre-1980 volcano, removed a volume of some 2.6 km^3 from it, and lowered its height by about 400 m (Moore and Albee 1981, p. 134). Subsequent dome growth has restored a volume of ~ 0.08 km^3 (Swanson and Holcomb 1990). The ultimate effect on the eruptive behavior of the volcano, if any, of the subtraction and addition of such volumes is not yet known. The volcano is underlain by a deep (>7 km) reservoir of volatile-rich magma that vents intermittently to the surface, apparently through a narrow conduit system. The upper levels of the conduit have been the source for most, but possibly not all, dome-building eruptions since 1980. Dacite erupted during 1980–1986 shows a chemical cycle of decreasing then increasing silica contents with time, similar to that in the Goat Rocks eruptive period. The current chemical cycle appears to be virtually complete; however, changes in seismicity since 1987 indicate the conduit system is under stress. Continuing seismicity and small explosions from the dome indicate that additional eruptive activity is still possible within the next few years.

The volcano's present shape, with a deep crater open to the north, will probably channel lava flows, pyroclastic flows, and lahars in that direction until the crater is filled. We believe that Mount St. Helens basically is still a growing volcano and that future eruptions will restore the roughly symmetrical shape it had before 1980. There is no confident way of forecasting whether this will occur within the next few decades or in the more distant future.

The potentially most destructive eruptions are those that involve large volumes of volatile-rich magma, and at least five major explosive eruptions occurred at Mount St. Helens over the 510 years since the start of the Kalama period (Hoblitt et al. 1980; Mullineaux and Crandell 1981; Mullineaux 1986; Crandell 1987). Three of these took place during the Kalama eruptive period, and one initiated the Goat Rocks period; the fifth was the eruption on 18 May 1980. Averaging these five eruptions over the 510 years since the start of the Kalama period suggests about a 1% annual probability of such an eruption.

Acknowledgments. We wish to express appreciation to TJ Casadevall, D Dzurisin, TM Gerlach and PW Lipman, who made many suggestions for improving an early version of the manuscript based on their personal knowledge of Mount St. Helens and its hazards. We thank RJ Knight for careful and expeditious INAA analyses, G Van Trump for providing geochemical data base support, JE Taggart for providing major-element XRF analyses, and GP Meeker for microprobe assistance. Discussions with SR Brantley, KV Cashman, CW Criswell, SD Malone, DA Swanson, and EW Wolfe about the current eruptive episode, PT Delaney about magma conduits, TM Gerlach about gas emissions, and CA Hopson about the Kalama eruptive period are gratefully acknowledged. We also appreciate constructive manuscript reviews and suggestions by WP Leeman, JM Rhodes, MJ Rutherford, and an anonymous reviewer for *Bulletin of Volcanology*. We especially thank executive editor G Mahood for manuscript handling and for an exceptionally thoughtful and careful review of the revised manuscript.

Appendix

Analytical methods and data sources

Major element oxide data presented herein were determined by X-ray fluorescence methods by JE Taggart, AJ Bartel, and DF Siems of USGS. Trace elements were determined using INAA methods by RJ Knight of USGS. Analytical methods are described by Taggart et al. (1987) and Baedecker and McKown (1987). The analytical data presented here for the Kalama and Goat Rocks eruptive periods are part of a geochemical database

acquired by the authors in collaboration with JE Taggert, DS Siems, and RJ Knight of USGS. Analytical data for the current eruptive period are mainly from rock samples in the collection of the D.A. Johnston Cascades Volcano Observatory and were extracted from computer-tape archives of the USGS Branch of Geochemistry by George Van Trump.

References

Baedecker PA, McKown DM (1987) Instrumental neutron activation analysis of geochemical samples. In: Baedecker PA (ed) Methods for geochemical analysis. US Geol Surv Bull 1770. H1-H14

Bard JP (1983) Metamorphism of an obducted island arc: example of the Kohistan sequence (Pakistan) in the Himalayan collided range. Earth Planet Sci Lett 45:133-144

Barker SE, Malone SD (in press) Magmatic system geometry at Mount St Helens modeled from the stress field associated with post-eruptive earthquakes. J Geophys Res

Bennett JT, Krishnswami S, Turekian KK, Melson WG, Hopson CA (1982) The uranium and thorium decay series nuclides in Mt St Helens effusives. Earth Planet Sci Lett 60:61-69

Blake S, Ivey GN (1986a) Magma-mixing and the dynamics of withdrawal from stratified reservoirs. J Volcanol Geotherm Res 27:153-178

Blake S, Ivey GN (1986b) Density and viscosity gradients in zoned magma chambers, and their influence on withdrawal dynamics. J Volcanol Geotherm Res 30:210-230

Boden DR (1989) Evidence for step-function zoning of magma and eruptive dynamics, Toquima caldera complex, Nevada. J Volcanol Geotherm Res 37:39-57

Carey S, Sigurdsson H (1985) The May 18, 1980 Eruption of Mount St Helens 2. Modeling of dynamics of the Plinian Phase. J Geophys Res 90:2948-2958

Carey S, Gardner J, Sigurdsson H (1989) Intensity and magnitude of post-glacial Plinian eruptions at Mount St Helens (abst). In: Continental magmatism. New Mexico Bureau of Mines and Mineral Resources Bull 131:43

Carey S, Sigurdsson H, Gardner JE, Criswell W (1990) Variations in column height and magma discharge during the May 18, 1980 eruption of Mount St Helens. J Volcanol Geotherm Res 43:99-112

Carroll MR, Rutherford MJ (1987) The stability of igneous anhydrite: experimental results and implications for sulfur behavior in the 1982 El Chichon trachyandesite and other evolved magmas. J Petrol 28:781-801

Casadevall TJ, Johnston DA, Harris DM, Rose WI, Malinconico LL, Stoiber RE, Bornhorst TJ, Williams SN, Woodruff L, Thompson JM (1981) SO_2 emission rates at Mount St Helens from March 29 through December, 1980. US Geol Surv Prof Paper 1250:193-207

Casadevall TJ, Rose W, Gerlach T, Greenland LP, Ewert J, Wunderman R, Symonds R (1983) Gas emissions and the eruptions of Mount St Helens through 1982. Science 221:1383-1384

Cashman KV (1988) Crystallization of Mount St Helens 1980-1986 dacite: a quantitative textural approach. Bull Volcanol 50:194-209

Cashman KV, Taggart JE (1983) Petrologic monitoring of 1981 and 1982 eruptive products from Mount St Helens. Science 221:1385-1387

Chadwick WW Jr, Swanson DA, Iwatsubo EY, Heliker CC, Leighley TA (1983) Deformation monitoring at Mount St Helens in 1981 and 1982. Science 221:1378-1380

Chadwick WW Jr, Archuleta RJ, Swanson DA (1988) The mechanics of ground deformation precursory to dome-building extrusions at Mount St Helens 1981-1982. J Geophys Res 93:B5:4351-4366

Christiansen RL, Peterson DW (1981) Chronology of the 1980 eruptive activity. US Geol Surv Prof Paper 1250:17-30

Crandell DR (1976) Preliminary assessment of potential hazards from future volcanic eruptions in Washington. US Geol Surv Misc Field Studies Map MF-774

Crandell DR (1980) Recent eruptive history of Mount Hood, Oregon, and potential hazards from future eruptions. US Geol Surv Bull 1492:1-81

Crandell DR (1987) Deposits of pre-1980 pyroclastic flows and lahars from Mount St Helens volcano, Washington. US Geol Surv Prof Paper 1444:1-91

Crandell DR, Mullineaux DR (1978) Potential hazards from future eruptions of Mount St Helens. US Geol Surv Bull 1383-C:1-26

Criswell CW (1987) Chronology and pyroclastic stratigraphy of the May 18, 1980 eruption of Mount St Helens, Washington. J Geophys Res 92:10237-10266

Criswell CW (1989) Volumes and compositional variations of the May 18, 1980 eruption of Mount St Helens: implications for eruption forecasts (abst). In: Continental magmatism. New Mexico Bureau of Mines and Mineral Resources Bull 131:62

Delaney PT, Pollard DD, Ziony JI, McKee EH (1986) Field relations between dikes and joints: emplacement processes and paleostress analysis. J Geophys Res 91:4920-4938

Devine JD, Sigurdsson H, Davis AN, Self S (1984) Estimates of sulfur and chlorine yield to the atmosphere from volcanic eruptions and potential climate effects. J Geophys Res 89:6309-6325

Dvorak J, Okamura AT, Mortensen C, Johnson MJS (1981) Summary of electronic tilt studies at Mount St Helens. US Geol Surv Prof Paper 1250:169-174

Endo ET, Dzurisin D, Murray T, Syverson K (1987) The rate of magma ascent during dome-building at Mount St Helens (abst). Abstract volume, Hawaii Symposium on How Volcanoes Work:64

Endo ET, Dzurisin D, Swanson DA (1990) Geophysical and observational constraints for ascent rates of dacitic magma at Mount St Helens. In: Ryan MP (ed) Magma transport and storage. Wiley, New York, pp-317-334

Evarts RC, Ashley RP, Smith JG (1987) Geology of the Mount St Helens area: record of discontinuous volcanic and plutonic activity in the Cascade arc of southern Washington. J Geophys Res 92:10155-10169

Fink JH, Malin MS, Anderson SW (1990) Intrusive and extrusive growth of the Mount St Helens lava dome. Nature 348:435-437

Gerlach TM, Casadevall TJ (1986) Fumarole emissions at Mount St Helens volcano, June 1980 to October 1981; degassing of a magma-hydrothermal system. J Volcanol Geotherm Res 28:141-160

Gerlach TM, Westrich HR, Casadevall TJ (1990) High sulfur and chlorine magmas during the 1989-90 eruption of Redoubt volcano, Alaska (abst). Am Geophys Union Trans (EOS) 71:1702

Glicken H, Meyer W, Sabol M (1989) Geology and ground-water hydrology of Spirit Lake blockage, Mount St Helens, Washington, with implications for lake retention. US Geol Surv Bull 1789:1-33

Halliday AN, Fallick AE, Dickin AP, Mackenzie AB, Stephens WE, Hildreth W (1983) The isotopic and chemical evolution of Mount St Helens. Earth Planet Sci Lett 63:241-256

Heliker CC (1984) Inclusions in the 1980-83 dacite of Mount St Helens, Washington. MSc thesis, Western Washington University:1-185

Hill PM, Rutherford MJ (1989) Experimental study of amphibole breakdown in Mount St Helens dacite with applications to magmatic ascent rate determinations (abst). New Mexico Bureau of Mines and Mineral Resources Bull 131:131

Hoblitt RP (1989) Day 3: The Kalama eruptive period, southwest and south flanks. In: Field excursions to volcanic terranes in the western United States II: Cascades and Intermountain West. New Mexico Bureau of Mines and Mineral Resources Memoir 47:65-69

Hoblitt RP, Crandell DR, Mullineaux DR (1980) Mount St Helens eruptive behavior during the past 1,500 yr. Geology 8:555–559

Hoblitt RP, Miller CD, Vallance JW (1981) Origin and stratigraphy of the deposit produced by the May 18 directed blast. US Geol Surv Prof Paper 1250:401–419

Hopson CA, Melson WG (1980) Mount St Helens eruptive cycles since 100 A.D. (abst). American Geophysical Union Trans (EOS) 61:1132–1133

Hopson CA, Melson WG (1984) Eruption cycles and plug-domes at Mount St Helens (abst). Geol Soc Am Abst with Programs 16:544

Hopson CA, Melson WG (1990) Compositional trends and eruptive cycles at Mount St Helens. Geosci Can 17:131–141

Irvine TN (1967) The Duke Island ultramafic complex, southeastern Alaska. In: Wyllie PJ (ed) Ultramafic and related rocks. Wiley, New York, pp 84–96

Jaeger JC (1957) The temperature in the neighborhood of a cooling intrusive sheet. Am J Sci 255:306–316

James OB (1971) Origin and emplacement of the ultramafic rocks of the Emigrant Gap area, California. Jour Petrology 12:523–560

Leeman WP, Smith DR, Hildreth W, Palacz Z, Rogers N (1990) Compositional diversity of Late Cenozoic basalts in a transect across the southern Washington Cascades: Implications for subduction zone magmatism: J Geophys Res 95:19561–19582

Lees JM, Crosson RS (1989) Tomographic inversion for three dimensional velocity structure of Mount St Helens using earthquake data. J Geophys Res 94:5716–5728

Lipman PW, Mullineaux DR (eds) (1981) The 1980 eruptions of Mount St Helens, Washington. US Geol Surv Prof Paper 1250

Lipman PW, Moore JG, Swanson DA (1981a) Bulging of the north flank before the May 18 eruption – geodetic data. US Geol Surv Prof Paper 1250:143–156

Lipman PW, Norton DR, Taggart JE Jr, Brandt EL, Engleman EE (1981b) Compositional variations in 1980 magmatic products. US Geol Surv Prof Paper 1250:631–640

Malone SD (1990) Mount St Helens, the 1980 rewakening and continuing seismic activity. Geosci Can 17:146–149

Mellors RA, Waitt RB, Swanson DA (1988) Generation of pyroclastic flows and surges by hot-rock avalanches from the dome of Mount St Helens volcano, USA. Bull Volcanol 58:14–25

Melson WG (1983) Monitoring the 1980–1982 eruptions of Mount St Helens: compositions and abundances of glass. Science 221:1387–1391

Merzbacher C, Eggler DH (1984) A magmatic geohygrometer: application to Mount St Helens and other dacitic magmas. Geology 12:587–590

Miller CD, Mullineaux DR, Crandell DR (1981) Hazards assessments at Mount St Helens. In: Lipman PW, Mullineaux DR (eds) The 1980 eruptions of Mount St Helens, Washington. US Geol Surv Prof Paper 1250:789–802

Mooney WD, Weaver CS (1989) Regional crustal structure and tectonics of the Pacific coastal states; California, Oregon, and Washington. Geol Soc Am Mem 172:129–161

Moore, JG, Albee WC (1981) Topographic and structural changes, March-July 1980 – photogrammetric data. US Geol Surv Prof Paper 1250:123–134

Moran S, Malone SD (1990) Recent micro-seismic activity at Mt St Helens and its implications for the evolution of the deeper magmatic system (abst). Am Geophys Union Trans (EOS) 71:1693–1694

Mullineaux DR (1976) Preliminary map of volcanic hazards in the 48 conterminous United States. US Geol Surv Misc Field Studies Map MF-786

Mullineaux DR (1986) Summary of pre-1980 tephra-fall deposits erupted from Mount St Helens, Washington State, USA. Bull Volcanol 48:17–26

Mullineaux DR, Crandell DR (1981) The eruptive history of Mount St Helens. US Geol Surv Prof Paper 1250:3–15

Nakamura K (1977) Volcanoes as possible indicators of tectonic stress orientation – principle and proposal. J Volcanol Geotherm Res 2:1–16

Newhall CG (1982) A method for estimating intermediate- and long-term risks from volcanic activity, with an example from Mount St Helens, Washington. US Geol Surv Open-File Report 82-396:1–50

Pallister JS, Hoblitt RP (1985) Magma mixing at Mount St Helens (abst). Am Geophys Union Trans (EOS) 66:111

Pallister JS, Heliker C, Hoblitt RP (in press) Glimpses of the active pluton below Mount St. Helens (abst). Am Geophys Union Trans (EOS) 72

Pearce JA (1982) Trace element characteristics of lavas from destructive plate margins. In: Thorpe RS (ed) Andesites. Wiley, New York, pp 525–548

Rutherford MJ (1990) Experimental study of dehydration and crystallization produced by decompression of dacites: implications for magma ascent rates (abst). Goldschmidt Conf Prog Abst 78

Rutherford MJ, Devine JD (1988) The May 18 eruption of Mount St Helens. 3. Stability and chemistry of amphibole in the magma chamber. J Geophys Res 93 B10:11949–11959

Rutherford MJ, Sigurdsson H, Carey S, Davis A (1985) The May 18, 1980, eruption of Mount St Helens 1. Melt composition and experimental phase equilibria. J Geophys Res 90 B4:2929–2947

Sager JW, Chambers DR (1986) Design and construction of the Spirit Lake outlet tunnel, Mount St Helens, Washington. In: Schuster RL (ed) Landslide dams: processes, risk, and mitigation. Am Soc Civil Engineers Geotechnical Special Publication 3:42–58

Sarna-Wojcicki AM, Shipley S, Waitt RB Jr, Dzurisin D, Woods SH (1981) Areal distribution, thickness, mass, volume, and grain size of air-fall ash from the six major eruptions of 1980. US Geol Surv Prof Paper 1250:577–600

Scandone R, Malone SD (1985) Magma supply, magma discharge and readjustment of the feeding system of Mount St Helens during 1980. J Volcanol Geotherm Res 23:239–262

Scarfe CM, Fujii T (1987) Petrology of crystal clots in the pumice of Mount St Helens' March 19, 1982 eruption; significant role of Fe-Ti oxide crystallization. J Volcanol Geotherm Res 34:1–14

Shemeta JE, Weaver CS (1986) Seismicity accompanying the May 18, 1980 eruption of Mount St Helens, Washington. In: Keller SAC (ed) Mount St Helens: five years later. Eastern Washington University Press, Cheney, WA, 44–58

Sigurdsson H (1982) Volcanic pollution and climate: the 1783 Laki eruption. EOS Trans Am Geophys Union 63:601–602

Sillitoe RH (1973) The tops and bottoms of porphyry copper deposits. Econ Geol 68:799–815

Smith DR (1984) The petrology and geochemistry of High Cascade volcanics in southern Washington: Mount St Helens volcano and the Indian Heaven basalt field. Ph D dissertation, Rice University, Houston, Texas:1–409

Smith DR, Leeman WP (1982) Mineralogy and phase chemistry of Mount St Helens tephra sets W and Y as keys to their identification. Quat Res 17:211–227

Smith DR, Leeman WP (1987) Petrogenesis of Mount St Helens dacitic magmas. J Geophys Res 92. B10:10313–10334

Snoke AW, Sharp WD, Wright JE, Saleeby JB (1982) Significance of mid-Mesozoic periodotitic to dioritic intrusive complexes, Klamath Mountains-western Sierra Nevada, California. Geology 10:160–166

Spera FJ, Yuen DA, Greer JC, Sewell G (1986) Dynamics of magma withdrawal from stratified magma chambers. Geology 14:723–726

Stanley WD, Finn C, Plesha JL (1987) Tectonics and conductivity structures in the southern Washington Cascades. J Geophys Res 92:10179–10193

Swanson DA, Holcomb RT (1990) Regularities in growth of the Mount St Helens dacite dome, 1980–1986. In: Fink, JH (ed) Lava flows and domes. Springer, New York, pp 3–24

Swanson DA, Lipman PW, Moore JG, Heliker CC, Yamashita KM (1981) Geodetic monitoring after the May 18 eruption. US Geol Surv Prof Paper 1250:157–168

Swanson DA, Casadevall TJ, Dzurisin D, Malone SD, Newhall CG, Weaver CS (1983) Prediction of eruptions at Mount St Helens, June 1980 through December 1982. Science 221:1369–1376

Swanson DA, Dzurisin D, Holcomb RT, Iwatsubo EY, Chadwick WW, Casadevall TJ, Ewert JW, Heliker CC (1987) Growth of the lava dome at Mount St Helens, Washington (USA) 1981–1983. Geol Soc Am Sp Paper 212:1–16

Taggart JE, Lindsay JR, Scott BA, Vivit DV, Bartel AJ, Stewart KC (1987) Analysis of geologic materials by X-ray fluorescence spectrometry. In: Badecker PA (ed) Methods for geochemical analysis. US Geol Surv Bull 1770. pp E1–E19

Thompson RN, Morrison MA, Dicken AP, Hendry GL (1983) Continental flood basalts ... Arachnids rule OK? In: Hawkesworth CJ, Norey MJ (ed) Continental basalts and mantle xenoliths. Shiva, Cambridge MA, pp 158–185

US Army Corps of Engineers (1986) Mount St Helens, Washington – Toutle, Cowlitz and Columbia Rivers. Portland District, Sedimentation Design Memorandum 3

Waitt RB Jr, Pierson TC, MacLeod NS, Janda RJ, Voight B, Holcomb RT (1983) Eruption-triggered avalanche, flood, and lahar at Mount St Helens – Effects of winter snowpack. Science 221:1394–1397

Walsh JB (1975) An analysis of local changes in gravity due to deformation. Pure Appl Geophys 113:97–106

Weaver CS, Grant WC, Malone SD, Endo ET (1981) Post-May 18 seismicity: volcanic and tectonic implications. US Geol Surv Prof Paper 1250:109–122

Weaver CS, Zollweg JE, Malone SD (1983) Deep earthquakes beneath Mount St Helens: evidence for magmatic gas transport? Science 221:1391–1394

Weaver CS, Grant WC, Shemeta JE (1987) Local crustal extension at Mount St Helens, Washington. J Geophys Res 92:10170–10178

Williams DL, Abrams C, Finn C, Dzurisin D, Johnson DJ, Denlinger R (1987) Evidence from gravity data for an intrusive complex beneath Mount St Helens. J Geophys Res 92:10207–10222

Wright TL, Doherty PC (1970) A linear programming and least squares method for solving petrologic mixing problems. Geol Soc Am Bull 81:1995–2008

Yamaguchi DK (1983) New tree-ring dates for recent eruptions at Mount St Helens. Quat Res 20:246–250

Yamaguchi DK (1985) Tree-ring evidence for a two-year interval between recent prehistoric explosive eruptions of Mount St Helens. Geology 13:554–557

Yamaguchi DK (1986) Interpretation of cross correlation between tree-ring series. Tree-ring Bull 46:47–54

Yamaguchi DK, Lawrence DB, Hoblitt RP (1990) A new tree-ring date for Mount St Helens' "Floating Island" lava flow. Bull Volcanol 52:545–550

Editorial responsibility: GA Mahood